Journal of Molecular Structure 1240 (2021) 130581

Contents lists available at ScienceDirect

Journal of Molecular Structure

journal homepage: www.elsevier.com/locate/molstr

Multi-sensing response, molecular docking, and anticancer activity of donor–acceptor chalcone containing phenanthrene and thiophene moieties

Marwa N. El-Nahass [a,*], Tarek A. Fayed [a], Saleh Abd Elazim [a], Mohammed M. El-Gamil [b], Doaa F. Draz [a], Fathy Hassan [a,*]

[a] Department of Chemistry, Faculty of Science, Tanta University, Tanta 31527, Egypt
[b] Department of Toxic and Narcotic Drug, Forensic Medicine, Mansoura Laboratory, Ministry of Justice, Medico legal Organization, Egypt

ARTICLE INFO

Article history:
Received 25 February 2021
Revised 17 April 2021
Accepted 25 April 2021
Available online 1 May 2021

Keywords:
Chalcone
Solvatochromism
Organized assemblies
Optical sensor
Metal complexes
Anticancer activities

ABSTRACT

Donor–Acceptor (D–π–A) chalcone containing phenanthrene and keto-thiophenly moieties, abbreviated as **PhTPO**, was synthesized and characterized. The solvatochromic effect was investigated in different solvents of various polarities. The absorption and fluorescence spectra have shown bathochromic shifts from non-polar to polar solvents due to intramolecular charge transfer interactions. The fluorescence characteristics (fluorescence intensity, fluorescence maxima, and energy) of **PhTPO** are highly sensitive to the polarity of the solvents compared to the corresponding absorption spectra. In addition, the inclusion characteristic of **PhTPO** in different organized assemblies was studied. The spectral changes suggested that **PhTPO** would be useful to study the microenviromental polarity and evaluation of critical micelle concentrations of the studied surfactants. Reversible acidochromic behavior was observed after addition of H_2SO_4/NaOH with a significant color change. Further, the optical sensing response towards H^+, Co^{2+}, Ni^{2+}, Pb^{2+} and Cd^{2+} ions was investigated. Also, it responds well to the tested metal ions as reflected from the changes in both the absorption and emission spectra upon adding different concentrations of the metal salts. The solid complexes of **PhTPO** with Co^{2+}, Ni^{2+}, Pb^{2+} and Cd^{2+} were then synthesized and characterized. Depending on the magnetic moments results, the geometric structures were found to be octahedral and tetrahedral for paramagnetic Co^{2+}, and Ni^{2+} complexes, respectively, while they are diamagnetic for Pb^{2+} and Cd^{2+} complexes. Moreover, the geometry of **PhTPO** and its complexes were confirmed by the density functional theory (DFT) using $DMOL^3$ program. The binding affinity towards the epidermal growth factor receptor (EGFR) protein was also investigated by the Molecular Operating Environment (MOE) software. The anticancer activity was then evaluated against four different cell lines using MTT assay. The results suggest that the investigated **PhTPO** would be potential candidate for solvents polarity sensors, as a probe to characterize critical micelle concentrations of surfactants, and sensor for the studied metal ions and H^+ proton. In addition, [**PhTPO**–Ni^{2+}] and [**PhTPO**–Co^{2+}] complexes are good candidate for further antitumor activities studies owing to their potent cytotoxic and anticancer activities compared to the Pb^{2+} and Cd^{2+} complexes.

1. Introduction

Solvatochromic and charge transfer behaviors of Donor–Acceptor (D–π–A) probes have received a great attention owing to the growing interest in different fields [1,2]. These probes have used for determination of the solvents polarity [3], as colorimetric chemosensors for volatile organic compounds [4,5], photo- and electroluminescent materials in laser [6,7], switchable viscosity probes [8], dual-ion-switched molecular brakes [9], and dye sensitized solar cells [10–12]. Among all of them, the chemotypes are great of interest for both chemists and physicists owing to their high natural abundance, their easy synthesis, and their diverse biological activities [13,14]. Chalcone is one of the most important D–π–A chemotypes due to its photophysical and photochemical properties including; high fluorescence quantum yield, large Stokes shift, excellent light stability, and less toxicity [15,16]. Owing to all these characteristics, chalcone and its derivatives have been used extensively in optoelectronics such as photorefractive poly-

* Corresponding authors.
E-mail addresses: marwa.elnahas@science.tanta.edu.eg (M.N. El-Nahass), fathy.hassan@science.tanta.edu.eg (F. Hassan).

https://doi.org/10.1016/j.molstruc.2021.130581
0022-2860/

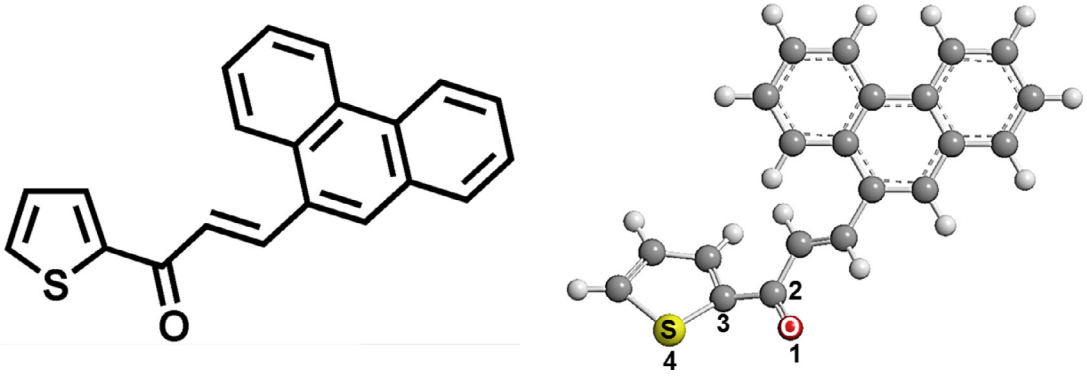

Scheme 1. Chemical structure and geometrical molecular model of phenanthrene-thiophene probe (**PhTPO**).

mers, nonlinear optical materials, DNA sensing, and in the study of photo-alignment layers in liquid crystals [17–20]. Further, chalcones have been used as anti-inflammatory, antibacterial, antitumor and antifungal owing to its biological activities [21–24]. In our laboratory, we have been focused on the application of chalcones as fluorescent probes for different metal ions sensing [25–28]. The high sensitivity towards the metal ions at low concentration levels suggested them as good candidates for toxic metal ions detection.

On the other hand, phenanthrene derivatives are a class of polycyclic aromatic hydrocarbon compounds that exhibited spectral and photophysical properties such as strong absorption cross section, excellent emission properties in both organic solutions and crystalline state, and large dipole moment in the exited state [29].

In this study, a new D–π–A chalcone namely 3-(phenanthren-9-yl)-1-(thiophen-2-yl)prop-2-en-1-one (**PhTPO**) was synthesized and characterized. The molecular design is composed of phenanthrene unit as an electron donor and keto-thiophene as an acceptor (Scheme 1). The solvatochromic effect was investigated in different solvents of various polarities. In addition, the inclusion characteristic in different surfactants was studied. Further, the optical sensing response to the H^+, Co^{2+}, Ni^{2+}, Pb^{2+} and Cd^{2+} ions was investigated. The solid complexes with Co^{2+}, Ni^{2+}, Pb^{2+}, and Cd^{2+} were also synthesized and characterized. The geometry of **PhTPO** and its complexes were confirmed by the density functional theory (DFT). The anticancer activity against four different cell lines using MTT assay was then evaluated.

2. Experimental

2.1. Materials

Unless otherwise noted, chemicals and solvents were purchased from commercial suppliers and were used as received without further purification. 2-Acetyl thiophene, 9-phenanthrenecarbaldehyde, sodium dodecyl sulfate (SDS), cetyltrimethylammonium bromide (CTAB), triton X-100 (TX-100), cobalt(II) chloride hexahydrate ($CoCl_2{\bullet}6H_2O$), nickel(II) chloride hexahydrate ($NiCl_2{\bullet}6H_2O$), lead(II) acetate trihydrate ($Pb(CH_3COO)_2.3H_2O$), cadmium chloride metal ($CdCl_2$,), methanol (MeOH), ethanol (EtOH), acetonitrile (ACN), dichloromethane (CH_2Cl_2), benzene (Benz), n-heptane (Hep), methylthiazolyldiphenyl-tetrazolium bromide (MTT), RPMI-1640 medium, and dimethyl sulfoxide (DMSO) were purchased from Sigma-Aldrich Chemicals. Fetal Bovine serum was purchased from GIBCO Fisher Scientific. All solvents were found to be non-fluorescent in the scanned range.

2.2. Methods

^{1}H- and ^{13}C NMR spectra were recorded on a Bruker 400 MHz NMR spectrometer using CDCl3 as a solvent. Chemical shifts are in δ unit (ppm) with the residual solvent peak as the internal standard. The coupling constant (J) is reported in hertz (Hz). NMR splitting patterns are designed as follows: *s*, singlet; *d*, doublet; *t*, triplet; *q*: quartet, and *m*, multiplet. The FT-IR spectra were recorded on JASCO FT-IR 4100 spectrophotometer using KBr technique within the range 4000–400 cm^{-1}. Mass spectra were measured on a Finnigan MAT 8222 EX mass spectrometer at 70 eV. Microanalysis of C, H, and S was carried out using a PerkinElmer 2400 elemental analyzer. The content of chloride and metal in investigated complexes were estimated as reported [30]. Thermogravimetric analysis (TGA) was performed using a Shimadzu TA-50 thermal analyzer under nitrogen atmosphere within a temperature range from 25 to 800 °C at a heating rate of 20 °C min^{-1}. Small-angle powder X-ray diffraction (XRD) measurements were done at room temperature using a GNR, APD 2000 PRO step scans X-ray diffractometer, with Cu Kα radiation (40 kV, 30 mA), and scanning range of 0–80° (2θ), with a step of 0.02°. Steady-state absorption and emission spectral measurements were carried out using a Shimadzu UV-3101 PC scanning spectrophotometer and Agilent Cary Eclipse Fluorescence Spectrophotometer, respectively. In all experiments, 2×10^{-5} M solutions were used and handled under dim light at room temperature. The fluorescence quantum yield (Φ_f) of the investigated probe was measured using the optically diluted solution to avoid the reabsorption effect (absorbance at excitation wavelength $\leq$0.1), relative to the method with a solution of quinine sulfate in 0.5 mol/dm^3 H_2SO_4 (Φ = 0.55) [31].

2.3. Synthesis

2.3.1. Synthesis of *PhTPO*

The investigated **PhTPO** was synthesized via aldol condensation between equal molar ratio of 2-acetyl thiophene and 9-phenanthrenecarbaldehyde in alcoholic sodium hydroxide (25% v/v solution of ethanol in water). The solution mixture was stirred at room temperature for 12 h. The product was precipitated after acidification using HCl solution (0.5 M) and it then separated by filtration under suction. The crude product was purified by recrystallization from methanol yielded **PhTPO** as a green crystal, mp 184 °C. ^{1}H NMR ($CDCl_3$, 400 MHz, Fig. S1 (a)): δ = 7.22–7.24 (t, 1H, J = 8.8 Hz), 7.56–7.74 (m, 7H), 7.95–7.97 (m, 2H), 8.28–8.30 (d, 1H, J = 8 Hz), 8.68–8.76 (m, 2H). ^{13}C NMR ($CDCl_3$, 400 MHz, Fig. S1 (b)): δ = 122.71, 123.23, 123.45, 124.52, 124.92, 126.63, 127.06, 127.09, 127.81, 128.14, 128.41, 129.27, 130.30, 131.17, 132.09, 132.15, 133.78, 134.11, 141.79, 145.50, 181.91 ppm. FT-IR (ν cm^{-1}, Fig. S2): 3400, 3200, 1650, 1600, 1450, 1350, 1100, 950, 800, 720, 675. Anal. Calcd. for $C_{21}H_{14}OS$: C, 79.44; H, 4.67 and S, 10.60; Found: C, 79.41; H, 4.62 and S, 10.62. C, 79.04; H, 6.24; N, 5.42. Found: C, 78.93; H, 6.31; N, 5.33. The mass spectrum (Fig. S3) shows a molecular ion peak of **PhTPO** at m/z = 314.20.

2.3.2. Synthesis of [PhTPO-M] complexes

[**PhTPO**-M] complexes were synthesized by mixing two solutions of the appropriate metal ions and **PhTPO** in EtOH, (1 mmol) in (10 ml) and (1 mmol) in (30 ml), respectively. The resulting mixtures were stirred under reflux for 12 h. The complexes were precipitated after cooling. The solid complexes were filtered off, washed with diethyl ether, and dried under vacuum. The [**PhTPO**-M] complexes were characterized by FT-IR, mass spectroscopy, and thermogravimetric analysis.

2.4. Quantum chemical calculation

The computations were performed using the BIOVIA Materials Studio package [32,33] with $DMOL^3$ program [34]. The geometry for all structures were optimized with RPBE functional [35] which is the best computational exchange-correlation [36] based on the generalized gradient approximation (GGA). The quantum calculation was obtained using the DFT semi-core pseudopod computations (dspp) with plus polarization of double numeric basis sets (DNP) [37–39].

2.5. Biological activities

2.5.1. Cytotoxic activity

PhTPO and its metal complexes were tested as prototypes for screening against a panel of four different human tumor cell lines: hepatocellular carcinoma (HePG-2), mammary gland (MCF-7), Human prostate cancer (PC3), and Colorectal carcinoma (HCT-116). The cell lines were obtained from ATCC via Holding company for biological products and vaccines (VACSERA), Cairo, Egypt. Doxorubicin was used as a standard anticancer drug for comparison. The different cell lines mentioned above were used to determine the inhibitory effects of the tested compounds on cell growth using the MTT assay. This colorimetric assay is based on the conversion of the yellow tetrazolium bromide of MTT to a purple formazan derivative by mitochondrial succinate dehydrogenase in viable cells. The cells were cultured in RPMI-1640 medium with 10% fetal bovine serum. Antibiotics added were 100 units/ml penicillin and 100 µg/ml streptomycin at 37 °C in a 5% CO_2 incubator. The cells were seeded in a 96-well plate at a density of $1.0 \times 1\ 0^4$ cells/well at 37 °C for 48 h under 5% CO_2 [40]. After incubation the cells were treated with different concentration of compounds and incubated for 24 h. After 24 h of drug treatment, 20 µl of MTT solution at 5 mg/ml was added and incubated for 4 h. DMSO in volume of 100 µl is added into each well to dissolve the purple formazan formed. The colorimetric assay is measured and recorded at absorbance of 570 nm using a plate reader (EXL 800, USA). The relative cell viability in percentage was calculated as (A570 of treated samples/A570 of untreated sample) x 100 [41].

2.5.2. . ABTS free radical and scavenging activity

The antioxidant activity assay by ABTS technique is carried out on each investigated compound as described previously [42–44].

2.5.3. . Antioxidant activity screening assay for erythrocyte hemolysis

The antioxidant activity screening for erythrocyte hemolysis is performed on the prepared compound as previously published literature [45,46].

2.6. . Molecular docking

Numerous studies have shown that the epidermal growth factor receptor (EGFR) is a potential therapeutic target for the treatment of various tumors, like colorectal and breast tumors [47]. Inactivation of this receptor could affect the spread of cell cancer and enhance apoptosis of cancer cells. For such a reason, we looked at the potential inhibitory effect of PhTPO and its metal complexes.

The Molecular Operating Environment (MOE) software was used to estimate binding affinity between EGFR protein and investigated compounds [48]. The MOE energy minimization algorithm with default parameters was used to minimize the energy of all 3D compound structures. Then, the charges on atoms were rendered and also the potential energy has been adjusted after minimization. The oriented investigated compound was stored in MDB-format as a new data base [49]. The crystal structure of EGFR receptor (PDB:3W2S) was obtained from Protein Data Bank (PDB) [50]. MOE was used to set up protein structures for molecular docking by eliminating ligand, adding hydrogen and minimizing 3W2S energy. The energy minimized structure was used as a docking receptor. The largest active site of 3W2S (LEU 718, VAL 726, LYS 745, GLY 719, ARG 841, ASP 855, and PHE 723) was obtained using the MOE site finder algorithm. The docking was produced using different features (initial re-scoring methodology: London dG with poses 10, final re-scoring methodology: GBVI/WSA dG with poses 5, placement: triangle matcher, and refining: rigid receptor) to identify and evaluate the connection between the prepared compounds and 3W2S. The most effective hits were chosen based on the inhibitor's S-score and root-mean-square deviation (RMSD) values. The S value is a score value that measures the affinity of the compound to the receptor and is computed by default score-built function of the MOE. While RMSD is also used to compare docked conformation with reference docked configuration. Retrieved compounds with higher S-value and lower RMSD value may be established as a potential inhibitor [51].

Table 1
Maximum absorption and fluorescence wavelengths, fluorescence quantum yields, and ground and excited states dipole moments of **PhTPO** in different solvents at 25 °C.

Solvent	λ^a_{max} (nm)	λ^f_{max} (nm)	Φ_f	$\mu_{g\ (D)}$	$\mu_{e\ (D)}$
Hep	351	410	0.002	4.42	28.4
Benz	356	422	0.004		
CH_2Cl_2	358	496	0.099		
ACN	357	462	0.023		
MeOH	361	501	0.021		
EtOH	364	491	0.025		

[a]: absorption
[f]:fluorescence

3. Results and discussion

3.1. Solvatochromic behaviors

Steady state absorption and fluorescence spectra of **PhTPO** have been studied in solvents of different polarities at room temperature (Fig. 1) and the corresponding spectroscopic data were summarized in Table 1. The absorption spectra of **PhTPO** showed broad structured band due to the localization of the transition Fig. 1(a). This was due to the interaction between the donor and acceptor molecular parts which has a small twisting of 10.51° in the torsion angle between O1, C2, C2, and S4 is, as shown in the geometrical structure of Scheme 1. The absorption spectra of **PhTPO** are less sensitive to the solvent polarity compared to the fluorescence spectra, indicating that its excited singlet states have high polar characters than its ground state. Fig. 1(b) represents the emission spectra of **PhTPO** in the studied solvents. The fluorescence spectra show a strong bathochromic shift as the solvent polarity is increased (ca. 91 nm) on going from Hep to MeOH, confirming the intramolecular charge transfer (ICT) of the excited state where charge transfer from the phenanthryl moiety to the carbonyl group takes place. This is accompanying by large difference in the

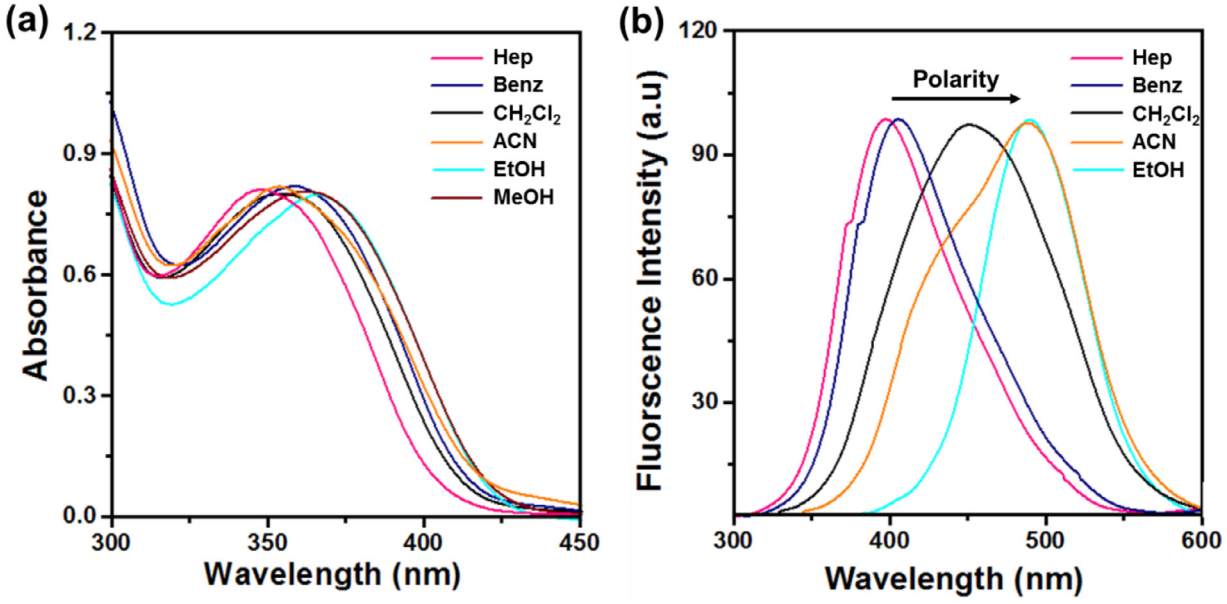

Fig. 1. Absorption (a) and emission (b) of **PhTPO** in different solvents.

dipole moment between the excited state and the ground state, $\Delta\mu = 23.98$ D.

The fluorescence properties of **PhTPO** were examined after UV irradiation (Fig. S4). **PhTPO** shows an interesting feature upon excitation at 365 nm in all of the used solvents. An intense emission was observed owing to the fluorescence characteristics of **PhTPO**.

The ground and excited states dipole moments were determined using Bakhshiev's and Kawski–Chamma–Viallet's equations [52]. The Onsager cavity radius, *a*, was estimated following geometry optimization of the investigated probe (with the help of ArgusLab 4.0 software and free HyperChem 8.03 software using PM3 Hamiltonian method) and comes out to be 5.5 A°. The dipole moments of **PhTPO** in both ground and excited states have been calculated and summarized in Table 1. The obtained values reveal that the dipole moments of the ground state is smaller than that in the excited state, confirming the existence of more than one of the relaxed polar excited state due to ICT favored by the cooperative effects of the phenanthryl moiety as a donor and the ketotheophenyl unit as an acceptor. These results suggest that the investigated **PhTPO** would be useful for nonlinear optical material. Also, the fluorescence quantum yield (Φ_f) is highly sensitive to the solvent effect (Table 1). The Φ_f values increase by 10.5 folds on going from Hep to MeOH confirming the strong ICT interaction.

Single crystals of **PhTPO** probe were obtained by slow evaporation of CH_2Cl_2 solution at room temperature for 3 days (Fig. 2(a)). The crystal structure was supposed to be owing to the π-π staking interaction of the phenanthrene units. Further study to assess the structure of single crystals is needed. However, the crystals were investigated under transmitting light using Optica Transmitted Microscope attached with Canon digital camera (Fig. S5) and the powder X-Ray diffraction patterns were shown in Fig. 2(b). The sharp peaks of the XRD patterns indicate the highly crystalline nature of **PhTPO**. The maximum counts are obtained at $2\theta = 25.85°$ with the count rate of 1168.

3.2. Effect of surfactants

The spectral properties of **PhTPO** have been studied in cationic CTAB, anionic SDS, and neutral TX-100 micellar media. Figure S6 shows the absorption and fluorescence spectra of **PhTPO** in different concentrations of the used surfactant and the corresponding spectral data are collected in Table 2. It was found that the absorption spectra increase with increasing the concentrations of the used surfactants with hypsochromic shift. The maximum absorption wavelength of **PhTPO** is shifted upon addition of CTAB, SDS, and TX-100. The quenching in the fluorescence intensities upon increasing surfactants concentration could be ascribed to the association of **PhTPO** with the surfactant. It seems that the **PhTPO** molecules located at the micelle–water interface showing the quenching role of water.

Table 2
Maximum absorption and fluorescence wavelengths of **PhTPO** in micellar solutions of the studied surfactants and their CMCs.

Surfactant	λ^a_{max} (nm)	λ^f_{max} (nm)	CMC $\times 10^{-3}$ (mol/L)
CTAB	370	525	3.7
TX-100	362	494	2.8
SDS	372	510	8.8

In order to examine the preferred conformation of **PhTPO** with the studied surfactants, the optimized molecular structures were evaluated to clarify the inclusion process. The optimized molecular structures were carried out in a simulation box (23.4 A × 60.0 A × 10.0 A). The low energy adsorption sites and the preferential geometries were optimized using Forcite classical simulation engine [53]. The supercell range was created using 6 layers of surfactants. As 3D periodic boundary conditions was used. Adsorption locator module in Materials Studio 2017 [54] was applied to model the adsorption and provide access to the energetic of the adsorption [55]. The binding energy between **PhTPO** and surfactants surface were calculated using the following equation [56].

$$E_{binding} = E_{total} - (E_{surface} + E_{adsorbate}) \quad (1)$$

where E_{total} is the total energy of the surface and **PhTPO**, $E_{surface}$ is the energy of the surfactant surface without **PhTPO**, and $E_{adsorbate}$ is the energy of **PhTPO** without the surfactant. A snap-shot of the individual conformation are presented in Fig. 3. It was expected that **PhTPO** show the highest ability to adsorb on surfactant surface owing to the high binding energy as seen in Table 3. The total energy is defined as the sum of the energies of the adsorbate components, the rigid adsorption energy and the deformation energy. In this study, the surfactant energy is taken as zero. The rigid adsorption energy reports the energy released (or required) when the unrelaxed adsorbate components (i.e., before the geometry op-

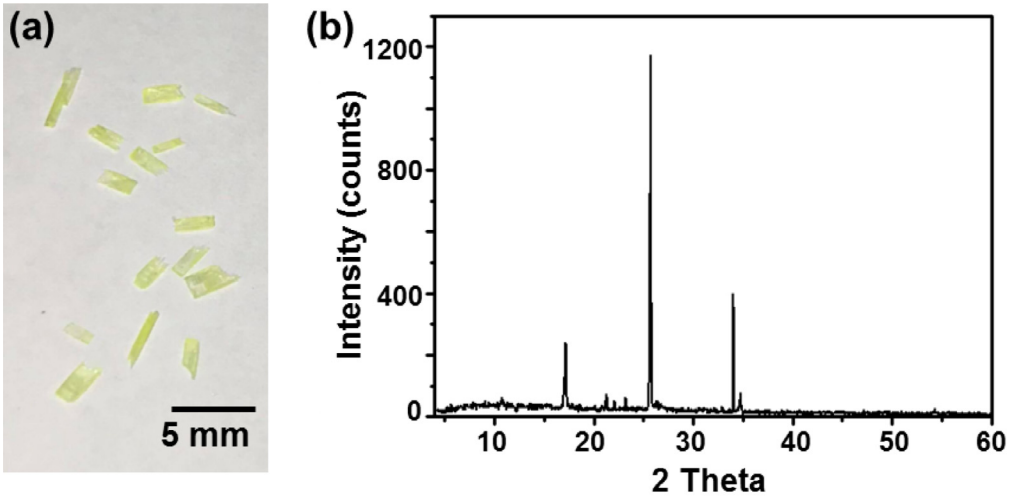

Fig. 2. Crystal structure of **PhTPO**; (a) image of the crystals, (b) XRD patterns.

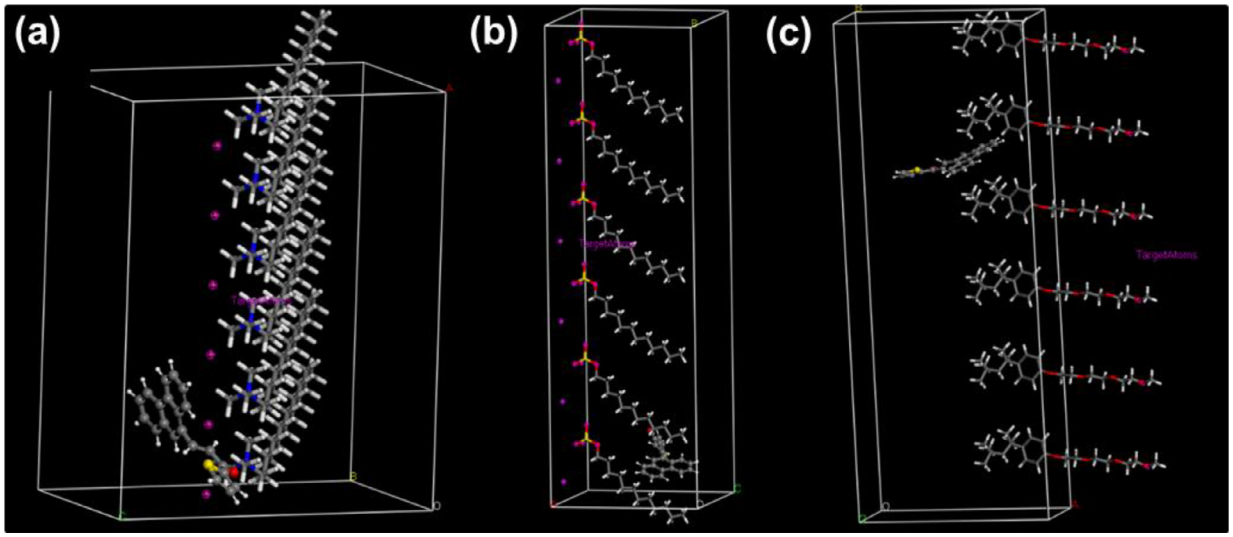

Fig. 3. The optimized stable conformers of the inclusion complexes between **PhTPO** and the studied surfactants; (a) CTAB, (b) SDS, and (c) TX-100.

Table 3
Calculated energy (by kcal mol^{-1}) for adsorption of **PhTPO** on surfactants surface.

Surfactant	Total energy	Adsorption energy	Rigid adsorption energy	Deformation energy	Binding Energy (kcal mol^{-1})
CTAB	63.166	−85.159	−75.603	−9.556	−156.355
SDS	102.986	−45.339	−36.022	−9.317	−116.535
TX–100	68.935	−79.389	−71.118	−8.271	−150.586

timization step) are adsorbed on the surfactant. The deformation energy reports the energy released when the adsorbent components are relaxed on the surfactant surface.

During the simulation process, **PhTPO** shows the maximum adsorption energy towards SDS and Triton-X-100 surfactants. High values of adsorption energy indicate that META derivative is the most efficient adsorption. The adsorption of **PhTPO** compounds can be described by physical adsorption which is the result of electrostatic attractive forces between the **PhTPO** and the surfactant surface.

3.3. Acidochromic behaviors

In order to study the sensing ability of PhTPO toward H^+ ions, the absorption and emission spectra were measured at different concentrations of sulfuric acid (Fig. 4). The absorption spectra were hanged dramatically upon increasing the concentration of sulfuric acid (from 10% to 98%) with an observable color change (Fig. S7). **PhTPO** solution changes from faint yellow, to red passing through faint pink when the concentration of sulfuric acid was increased. Interestingly, the initial faint yellow color is recovered upon the addition of sodium hydroxide solution or by dilution, which is an evidence for the reversibility of the prototropic equilibrium (Fig. 5). The fluorescence maximum of **PhTPO**, which appears at 496 nm, are blue-shifted by 11 nm at low sulfuric acid concentrations (from 10% to 40%), while it shows two bands at 414, and 588 nm at high concentrations (90%–98%) of sulfuric acid.

The possible mechanism of the effect of the acidity on the spectral characteristics of the investigated probe and sensitivity towards H^+ proton is shown in Scheme S1. It was expected that

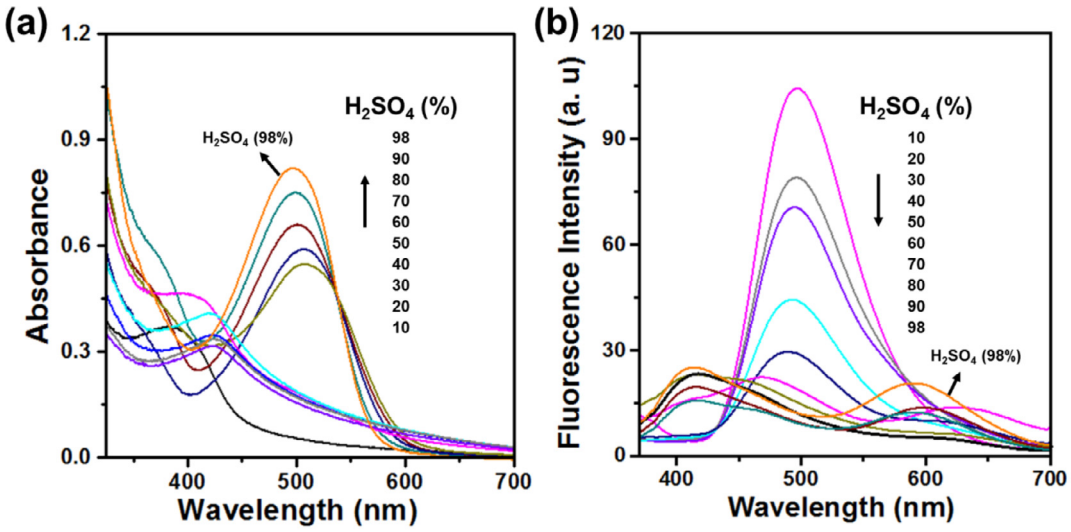

Fig. 4. Absorption (a) and emission (b) of **PhTPO** upon addition of different concentrations of sulfuric acid (For interpretation of the references to color in this figure, the reader is referred to the web version of this article.).

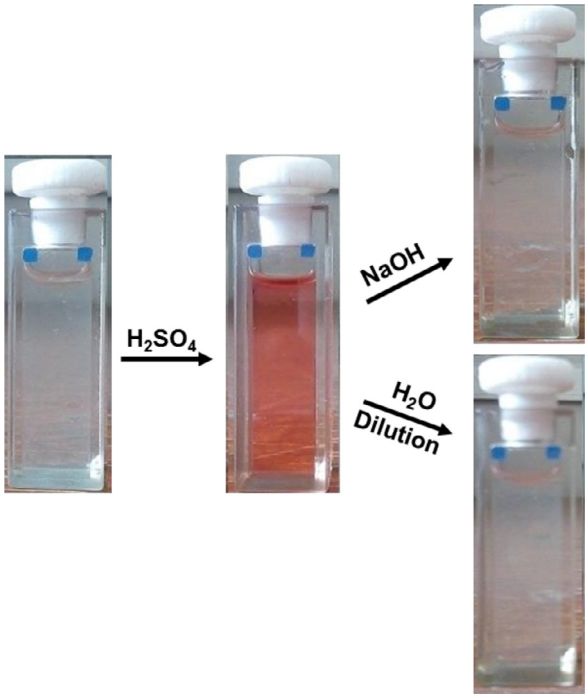

Fig. 5. Acidochromic behavior of **PhTPO** upon addition of H_2SO_4 and recovery to the initial state by addition of NaOH or dilution by H_2O (For interpretation of the references to color in this figure, the reader is referred to the web version of this article.).

there would be two protonation steps on adding sulfuric acid. The first step is the electrophilic addition of a proton to the high electron density oxygen of the carbonyl group giving resonance-stabilized adducts. Then, it was supposed a tautomeric structure leading to formation of isomer (I). The isomer (I) is due to the formation of the conjugated structure which would be obtained at concentrations of sulfuric acid within the range 10–40%, which is responsible for the blue shift. In contrary when the concentration of sulfuric acid increases, in the range 60–90%, isomer (II) was obtained, due to the protonation of both sulfur and oxygen atoms, and leads to the appearence of the red shifted absorption band. Both isomers are kinds of quinoid structure which is responsible for the color change after the protonation step which is possible to be recovered by addition of NaOH or by dilution. This reversible acidochromic behavior is promising as a colorimetric chemosensing technique in which detection approach of H^+ proton with naked eye. The pH responsive functional materials have broad applications including smart food packaging [57], wearable [58], food freshness monitoring [59], textilebased chemical sensors [60], and non-invasive bioprocess monitoring [61].

3.4. Metal ions sensing response

The sensing ability of **PhTPO** probe, towards metal ions; Co^{2+}, Ni^{2+}, Pb^{2+} and Cd^{2+} has been studied. Fig. 6 shows the absorption and emission spectra of the **PhTPO** in the presence of different concentrations of Co^{2+} and Ni^{2+}ions in EtOH.

After addition of Co^{2+} ions to 2×10^{-5} M **PhTPO** solution, the absorption maximum at 364 nm was decreases with appearance of a new absorption bands in the visible region at 509 and 637 nm. This was accompanied by formation of an isobestic point at 417 nm. Also, in case of adding Ni^{2+} salt solutions, the absorption maximum at 364 nm was decreases and a new band around 460 nm was developed with formation of an isosbestic point at 404 nm. On the other hand, on addition of Pb^{2+} ions, the absorption band of PhTPO at 364 nm increases gradually with appearance of a shoulder around 441 nm, while in case of Cd^{2+} ions the absorption at 364 nm decreases with slight bathochromic shift and buildup of a weak shoulder around 440 nm at higher concentrations. These changes were attributed to the formation of complexes between the used metal ions and the investigated probe via chelation with both sulfur atom of thiophene moiety and the oxygen of the carbonyl group.

Figure S8, shows the emission spectra of the investigated probe in the presence of different concentrations of the mentioned metal ions. As can be seen, the fluorescence band of PhTPO at 491 nm in EtOH, suffers slight hypsochromic shift on adding different concentrations of Co^{2+}, and Ni^{2+} ions, ca. 9, and 5 nm, respectively, with great quenching in the fluorescence intensity. In contrast, on adding different concentrations of Pb^{2+} or Cd^{2+} ions, the fluorescence intensity increases with detectable bathochromic shift, by ca. 15, and 17 nm, respectively. The quenching and turn-off of the fluorescence of PhTPO on adding of Co^{2+}, or Ni^{2+} salts could be assigned to the enhanced ligand to metal CT interactions supported by the open *d*-shell of these metal ions (d^7 and d^8 for Co^{2+}, and

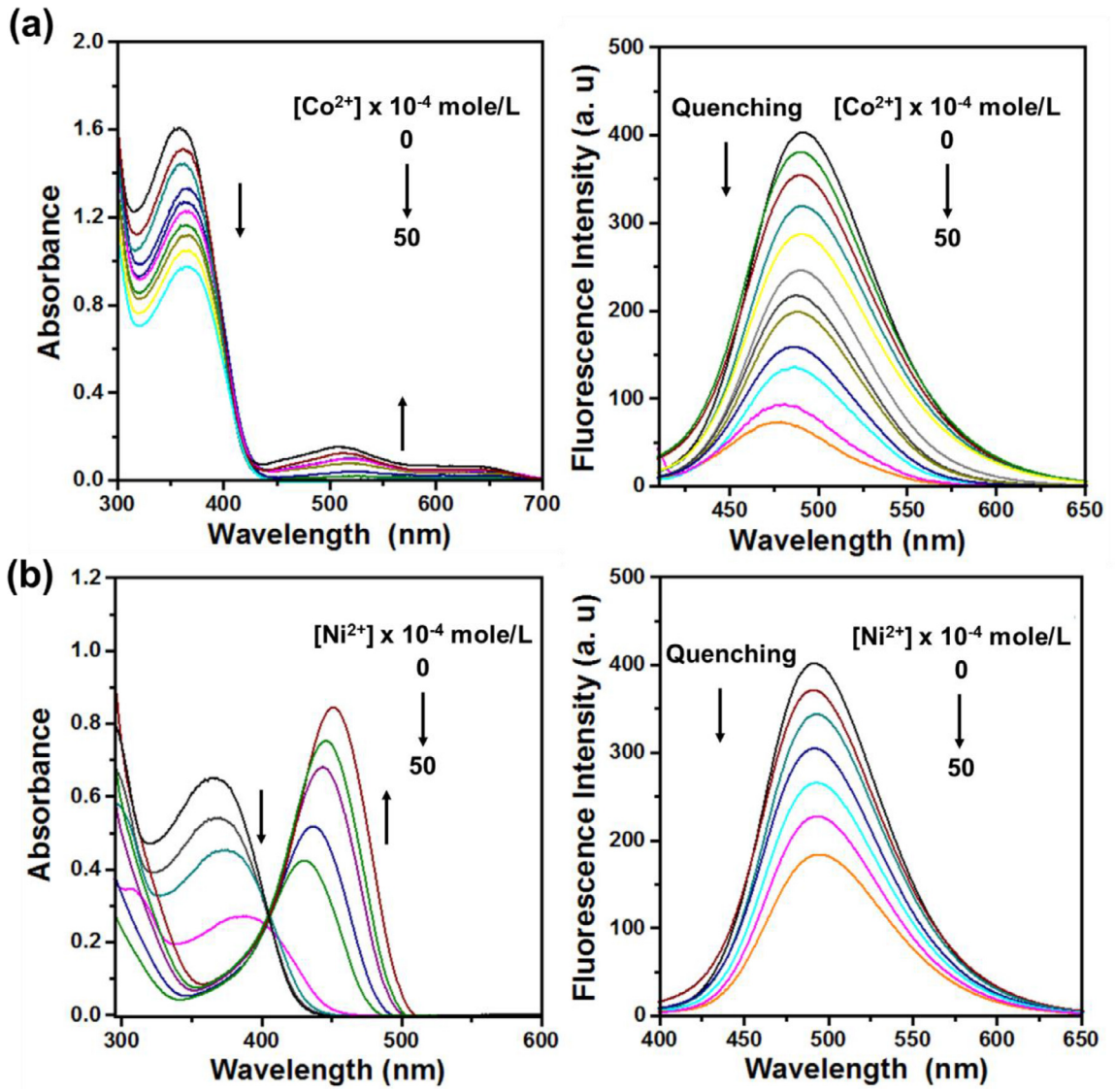

Fig. 6. Absorption and emission spectra of **PhTPO** upon addition of different concentrations of the studied metal ions; (a) Co^{2+} and (b) Ni^{2+}.

Ni^{2+} ion, respectively), which is confirmed by the buildup of a new intense absorption band in the visible region, especially in case of Ni^{2+} ions. In contrast, the turn-on and the enhancement in the fluorescence intensity on adding of Pb^{2+} or Cd^{2+} ions, were attributed to the absence of ligand to metal CT interactions where Pb^{2+} and Cd^{2+} ions have closed *d*-shell (d^{10}) and hindering of the radiationless free rotations in PhTPO molecules due to complex formation. The obtained results reflect the high sensitivity towards the used metal ions and recommend it as a promising switch optical sensor for detection of metal ions.

The stoichiometry between **PhTPO** probe and Co^{2+}, Ni^{2+}, Pb^{2+} and Cd^{2+} ions were performed using continuous variation method (Job's method). Fig. 7 shows the relation between the absorbance and the mole fraction C_L/C_L+C_M. It has been found that maxima occurs at 0.60, and 0.61 ratios of $Co^{2,}$ and Cd^{2+} ions concentration to the total Co^{2+}/ $Cd^{2+}$and **PhTPO** concentration indicating the formation of 1:2 (M:L) complex. However, the maxima at mole fractions of ca. 0.44, and 0.49 were obtained for Pb^{2+} and Ni^{2+} ions with **PhTPO** probe confirming 1:1 ratio.

The ground and excited state binding constants of Co^{2+}, Ni^{2+}, Pb^{2+}, and Cd^{2+}complexes with **PhTPO** were determined by employing Benesi–Hildebrand equation [62]. The binding constants (K) were calculated and summarized in Table 4 and Fig. S9. Fig. 8 shows the relation between the ground and excited state binding constants and the metal ions. The data reveal that the association constants of the metal ions with **PhTPO** sensor follows the order, Cd^{2+}> Co^{2+}> Ni^{2+}>Pb^{2+}. The high binding constants of both Cd^{2+} and Co^{2+} reveals the strong chelation between these metals and **PhTPO**.

Detection of this toxic species is worth to develop owing to their widespread occurrence in environment, causing a public health problem [63]. The investigated PhTPO is good candidate as a chemosensor for the detection of the studied metal ions with some

Table 4
Maximum absorption and fluorescence wavelengths, and ground and excited states association constants for the complexes between **PhTPO** probe and the metal ions in EtOH.

Compound	λ^a_{max}	λ^f_{max}	K_a (M^{-1})	K_f (M^{-1})
PhTPO	364	491	–-	–-
[**PhTPO**-Co^{2+}]	509, 637	482	524.20	692.50
[**PhTPO**-Ni^{2+}]	451	486	345.30	573.47
[**PhTPO**-Pb^{2+}]	441	506	217.50	245.30
[**PhTPO**-Cd^{2+}]	369	508	671.20	700.20

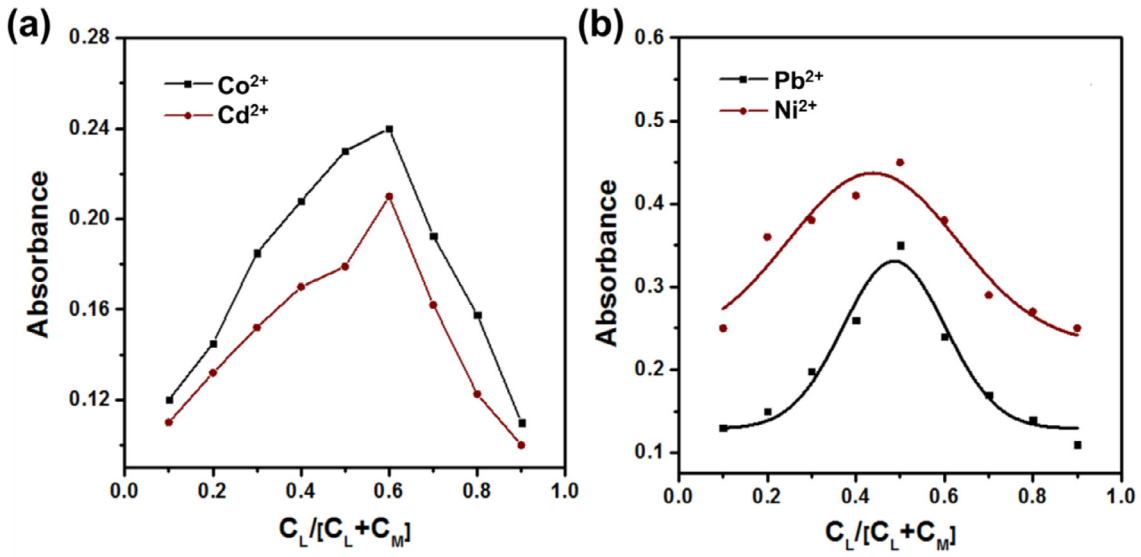

Fig. 7. Absorbance and mole fraction correlations; (a) for $Co^{2+}$and Cd^{2+}, (b) for $Pb^{2+}$and Ni^{2+}.

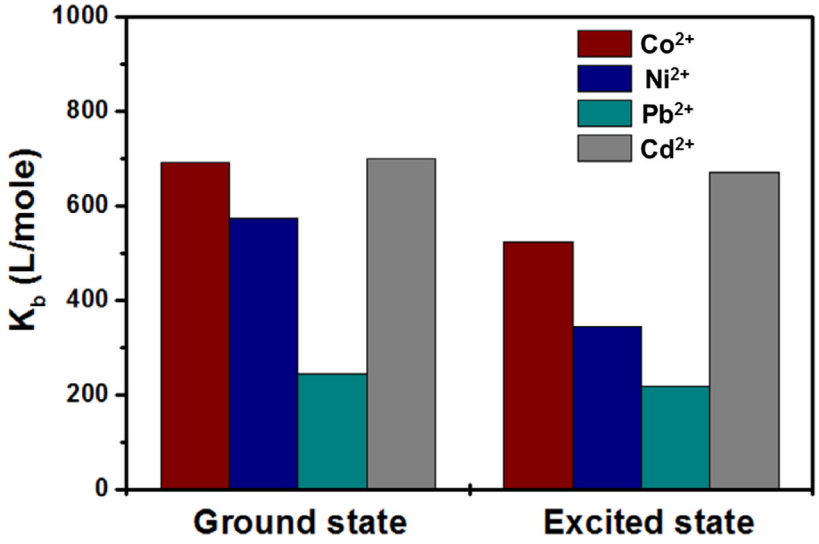

Fig. 8. The relation between the ground and excited state binding constants for the studied metal ions.

considerable characteristics using absorption and emission techniques. Such chemosensor is based on fluorescent materials which have attracted great attention because of advantages over conventional electrochemical approaches owing to ease of detection, fast response, simplicity, and high sensitivity [64]. The results show sensitivity within millimole level which would be useful for the detection of the studied toxic ions in industrial wastewater [65].

3.5. Structural characterization of the synthesized solid metal complexes

The results of elemental analysis of **PhTPO** probe and its Co^{2+}, Ni^{2+}, Pb^{2+}, and Cd^{2+} metal complexes along with their physical properties were collected in Table 5. The analytical data reveal 1:2 (metal-to-probe) stoichiometry for Co^{2+}, and Cd^{2+} complexes, while for Ni^{2+} and Pb^{2+}complexes it comes out to be 1:1. Based on these results, the corresponding probable constitutional formulae of the metal complexes were suggested as given in the same Table. The low molar conductance values of Co^{2+}, Ni^{2+}, and Pb^{2+} complexes (ΛM =7.9–14.5 $\Omega^{-1}cm^2$ mol^{-1}) measured in DMF solution, indicate the non-electrolytic nature of these complexes. However, the high molar conductance of Cd^{2+} complex confirms the electrolytic nature [66].

Fig. 9 shows the mass spectra of the probe [**PhTPO**-M] complexes. The obtained molecular ion peaks showed that m/z is equivalent to the molecular weight of the proposed complexes. The mass spectra of the complexes provided good evidence for their molecular formulae, $C_{42}H_{28}Cl_2CoO_2S_2$ (MW 758.64, m/z 758.33), $C_{22}H_{17}Cl_2NiO_{1.5}S$ (MW 467.03, m/z 467.06), $C_{25}H_{20}O_5PbS$ (MW 639.69, m/z 639.63), and $C_{56}H_{70}CdCl_2O_9S_2$ (MW 1134.60, m/z 983.59), respectively, and confirming the calculated stoichiometry of the formed complexes, where the ligand coordinates with Co^{2+}, and Cd^{2+} ions in 1:2 (M:L) ratio while for Ni^{2+} and Pb^{2+} it is 1:1. The lower m/z value of [**PhTPO**-Cd^{2+}] complex than the molecular weight of proposed formula because of the mass spectra measurements were carried out in the limited range from m/z 40 to 1000.

The structural confirmation of the metal complexes was confirmed by comparing the FT-IR spectrum of the investigated free **PhTPO** with those of the metal complexes, Fig. 10(a). Two main strong absorption peaks in the spectrum of **PhTPO** were observed at 1635, and 1225 cm^{-1}, due to ν(C = O) and ν(C–S), respectively. Comparing these frequencies with those of the metal complexes, it

Table 5
Analytical data of **PhTPO** and [**PhTPO**-M] complexes.

Compound	Color	Calcd. (Found)%				Λ_m ($\Omega^{-1}cm^2mol^{-1}$)	μ_{eff} (BM)
		C	H	S	M		
PhTPO	Orange	80.23	4.49	10.20	–-	–-	–-
$C_{21}H_{14}OS$; 314.40	yellow	(80.55)	(4.62)	(10.62)			
[**PhTPO**-$NiCl_2$].0.5C_2H_5OH	Brilliant	56.58	3.67	6.86	12.57	10.5	2.8
$C_{22}H_{17}Cl_2NiO_{1.5}S$; 467.03	green	(56.44)	(3.74)	(7.04)	(12.87)		
[(**PhTPO**)$_2$$CoCl_2$]	Faint Green	66.50	3.72	8.45	7.77	7.9	4.52
$C_{42}H_{28}Cl_2CoO_2S_2$; 758.64		(66.40)	(3.82)	(8.69)	(8.01)		
[**PhTPO**-$Pb(OAc)_2$]	Pale yellow	46.94	3.15	5.01	32.39	14.5	0
$C_{25}H_{20}O_5PbS$; 639.69		(46.88)	(3.19)	(5.10)	(32.46)		
[(**PhTPO**)$_2$Cd].Cl_2.7C_2H_5OH	Grayish	59.28	6.22	5.65	9.91	280	0
$C_{56}H_{70}CdCl_2O_9S_2$; 1134.60	green	(59.32)	(6.55)	(5.73)	(9.73)		

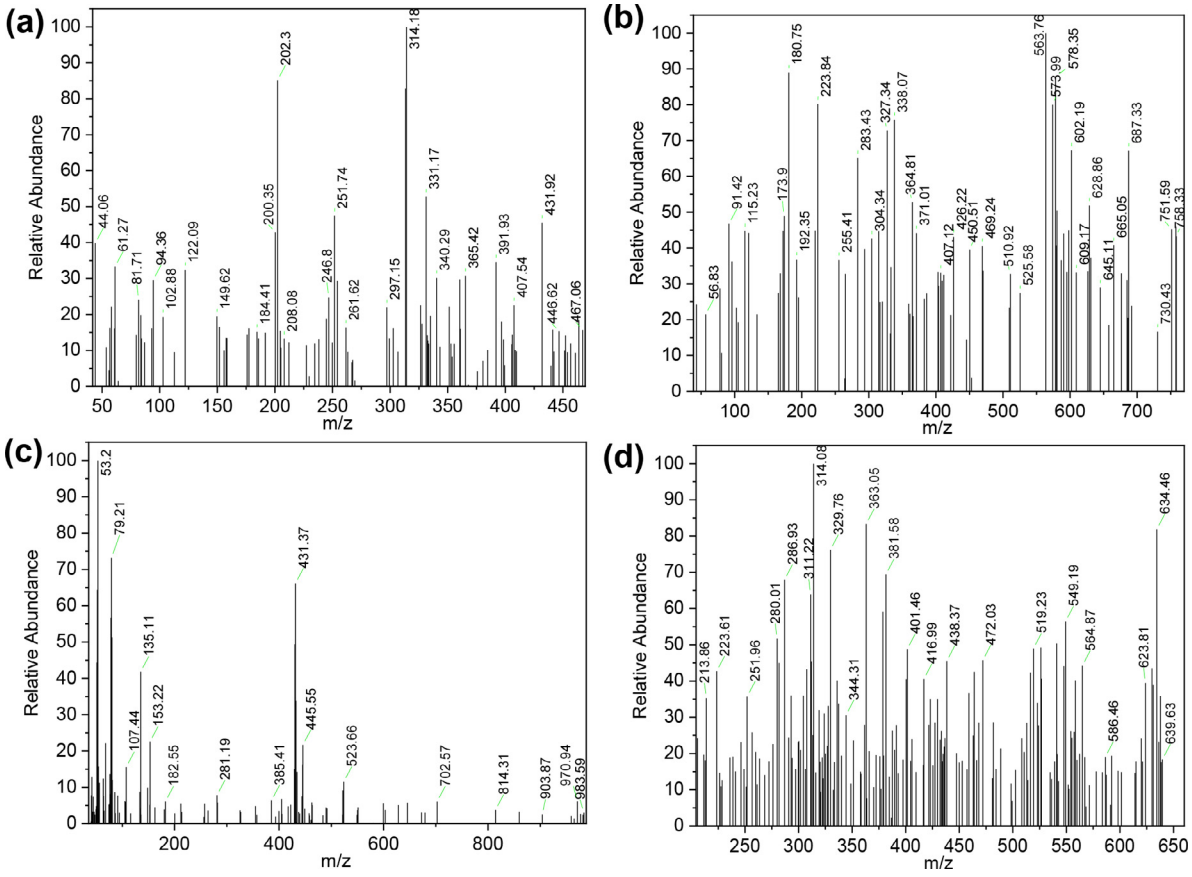

Fig. 9. Mass spectra of the investigated metal complexes; (a) [**PhTPO**-Ni^{2+}], (b) [**PhTPO**-Co^{2+}] (c) [**PhTPO**-Cd^{2+}], and (d) [**PhTPO**-Pb^{2+}].

was found that both ν(C = O) and ν(C–S) vibrational bands were shifted to lower and higher wavenumbers by 10– 42 for ν(C–O) and 6 – 11 cm^{-1} for ν(C–S), respectively. These shifts confirm the coordination of sulfur atom of thiophene moiety and the oxygen atom of the carbonyl group to the metal ions. Also, the complexes showed bands in the range 510–555 cm^{-1} assigned to ν(M–O) which could account for the presence of different stretching modes of M–O. Bands in the 416–466 cm^{-1} range were assigned as ν(M–S) stretching [67,68].

The thermal behavior of the synthesized metal complexes was investigated using TGA. The TGA thermograms of the metal complexes are shown in Fig. 10(b) and the data are collected in Table 6. The TG curve of [**PhTPO**-Co^{2+}] complex showed two steps. The first step in the region 25–390 °C has a mass loss of 67.18 (Calcd.67.95%), corresponding to decomposition of 2($C_{15}H_{10}S$) and Cl_2 (515.51). The second thermal process, in the region 390–800 °C, has a mass loss of 9.45 (Calcd. 9.87%), corresponding to further decomposition of the ligand leaving CoO residue (74.93).

The thermogram of [**PhTPO**-Ni^{2+}] complex showed three decomposition steps, the first one in the region 25–100 °C has a mass loss of 5.00 (Calcd. 4.93%), corresponding to decomposition of 1/2C_2H_5OH (23.03). the second step in the temperature range 100–380 °C with a mass loss 71.45 (Calcd. 71.16%), corresponding to decomposition of ($C_{18}H_{13}S$) and Cl_2 (332.36). The third step within the range 380–800 °C has a mass loss 15.65 (Calcd. 15.99%), corresponding to complete decomposition of the ligand leaving NiO residue (74.69). [**PhTPO**-Pb^{2+}] complex showed two decomposition steps with a mass loss of 41.25 (Calcd.41.32%) in the temperature range 25–410 °C, corresponding to decomposition of 2(CH_3CO) and $C_{14}H_{10}$ (264.31), and mass loss of 39.35 (Calcd. 39.27%) in the 410–800 °C range, consistent with complete decomposition of the ligand leaving PbO_2 and 1C residue (251.21). The TG curve of [**PhTPO**-Cd^{2+}] complex revealed an initial mass loss occurring within the

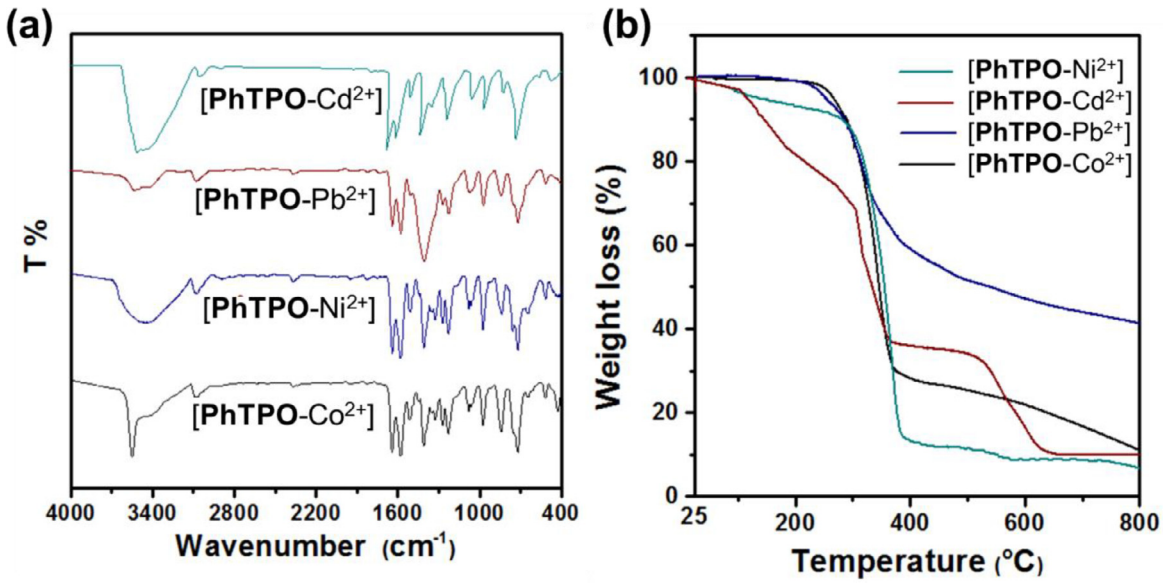

Fig. 10. FT-IR spectra (a) and TGA thermograms (b) of the investigated metal complexes.

Table 6
TGA analytical results of [**PhTPO-**M] complexes.

Complex	TG range (°C)	Decomposition product lost(Formula wt.)	Wt (%)Found (Calcd.)
[**PhTPO-**Co^{2+}]	25–390	$2(C_{15}H_{10}S) + Cl_2$	67.18 (67.95)
	390–800	(515.51) Further decomposition of ligand leaving CoO residue (74.93)	9.45 (9.87)
[**PhTPO-**Ni^{2+}]	25–100	$1/2C_2H_5OH$ (23.03)	5.00 (4.93)
	100–380	$(C_{18}H_{13}S) + Cl_2$	71.45 (71.16)
	380–800	(332.36) Further decomposition of ligand leaving NiO residue (74.69)	15.65 (15.99)
[**PhTPO-**Pb^{2+}]	25–410	$2(CH_3CO) + C_{14}H_{10}$	41.25 (41.32)
	410–800	(264.31) Further decomposition of ligand leaving PbO_2+ 1C residue (251.21)	39.35 (39.27)
[**PhTPO-**Cd^{2+}]	25–100	$7C_2H_5OH$ (322.48)	28.33 (28.42)
	100–400	$C_{28}H_{18}OCl_2$ (441.35)	38.56 (38.90)
	400–700	$2(C_7H_5S)$ (242.36)	21.47 (21.36)
	700–800	Residual metal oxide CdO (128.41)	11.17 (11.31)

temperature range 25–100 °C which was attributed to the loss of 7 C_2H_5OH, 28.33 (Calcd.28.42%). At higher temperature from 100 to 400 °C, loss of $C_{28}H_{18}OCl_2$ and Cl_2, 38.56 (Calcd 38.90%) occurred. A third decomposition step, in the 400–700 °C range, brought about a mass loss of 21.47 (Calcd 21.36%) corresponding to decomposition $2(C_7H_5S)$. The fourth step lying in the region 700–800 °C has a mass loss of 11.17 (Calcd.11.31%), g corresponding to the formation of stable CdO as revealed by the mass percentage of the end product.

The higher magnetic moment for [**PhTPO-**Co^{2+}] complex (μ_{eff}= 4.52 BM, suggests the high spin octahedral structure with sp^3d^2 hybridization, while the room temperature magnetic moment of [**PhTPO-**Ni^{2+}] complex is 2.8 BM which attributed to tetrahedral geometry. However, the diamagnetic nature of Pb^{2+} and Cd^{2+} complexes reveal sp^3 tetrahedral hybridization. Based on these results from the elemental analysis, conductivity, magnetic moment measurements and thermal studies, the proposed structures for the studied complexes were shown in Scheme S2.

3.6. Molecular modeling

3.6.1. Molecular electrostatic potential (MEP)

In this study, the three-dimensional structure of molecular electrostatic potential (MEP) of **PhTPO** and its Co^{2+}, Ni^{2+}, Pb^{2+}, and Cd^{2+} complexes have been represented (Fig. 11). The red and blue colors characterize regions of most positive electrostatic potential and most negative electrostatic potential, respectively. The potential increases with the order; red < orange < yellow < green < blue. From the MEP map, it can be revealed that the regions of negative potential are dispersed over the electronegative oxygen and sulfur atoms while that possessing positive potential are dispersed over the hydrogen atoms.

3.6.2. Geometry optimization

Comparing the data of bond distances and angles of **PhTPO** with that calculated for the prepared complexes, as summarized in Tables S1 and S2, the following points can be concluded: (1)

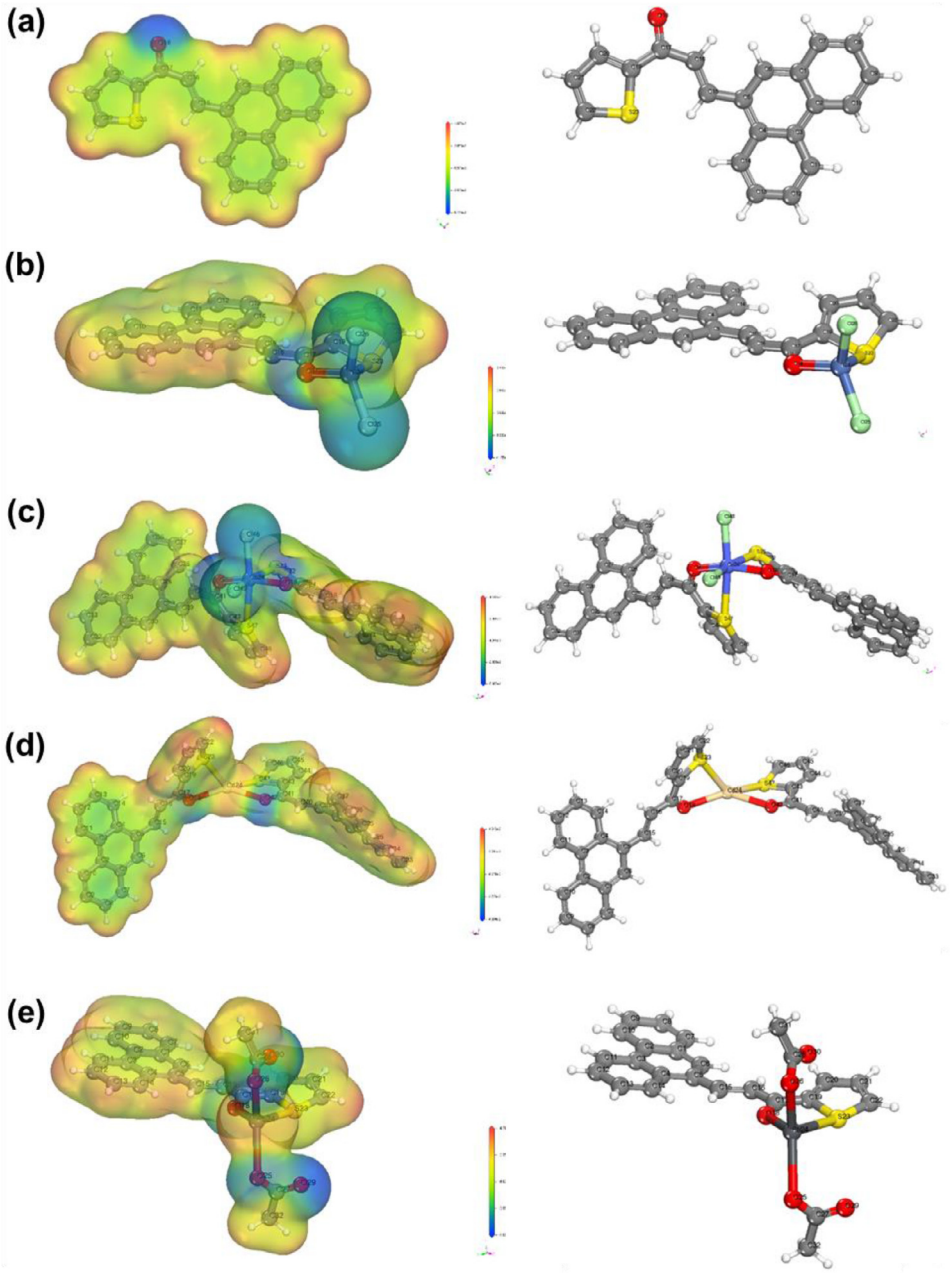

Fig. 11. Molecular surface of electrostatic potentioal and 3D geometry optimiztion structure of (a) **PhTPO**, (b) [**PhTPO-**Ni^{2+}], (c) [**PhTPO-**Co^{2+}], (d) [**PhTPO-**Cd^{2+}], and (e) [**PhTPO-**Pd^{2+}] (For interpretation of the references to color in this figure, the reader is referred to the web version of this article.).

The detected bond angles in Co^{2+} complex confirm an octahedral geometry with sp^3d^2 hybridization. While Ni^{2+}, Pb^{2+}, and Cd^{2+} complexes afforded the proposed tetrahedral geometry with sp^3 hybridization. (2) In all metal complexes, there is a great change in C(17)-O(18), C(19)-C(17) and C(19,22)-S(23) bond distances. They were changed to be slightly longer as the complexation with metal ion takes place *via* O atoms of the –C=O group [69]. Furthermore, the C(19,22)-S(23) bond lengths become longer as sulfur atom coordinates with metal which makes the C-S bond more fragile [70]. (3) Metal-oxygen bond is shorter than metal-sulfur bond telling the greater strength of M-O than M-S.

3.6.3. Global chemical reactivity

Frontier molecular orbital energy (Fig. 12) can assume effective coordination locations. The reaction is the result of overlap between the HOMO (highest occupied molecular orbital) of one molecule and the LUMO (lowest unoccupied molecular orbital) of the other. It is therefore possible to determine the chemical reactivity of the molecules under investigation. The energies of frontier molecular orbitals (E_{HOMO}, E_{LUMO}), chemical potential (μ), electronegativity (χ), global hardness (η), global electrophilicity index (ω), global softness (S) and additional electronic charge (ΔN_{max}) [71] are listed in Table 7. From the data obtained, the following points can be inferred: (1) Stability of the investigated molecules depends on the negative value of HOMO and LUMO energy levels [72,73]. (2) Depending on the energy gap values, soft and more active compounds have a minor change between the HOMO-LUMO levels. (3) Chemical potential 'μ' that estimate the ability of electrons to escape from the equilibrium system decreases with order Cd^{2+} complex (−3.443) > Co^{2+} complex (−3.740) > Ni^{2+} complex (−4.156) > **PhTPO** (−4.192)> Pb^{2+} complex (−4.229). (4) The calculation of reactivity index (ΔN_{max}) revealed that Cd^{2+} complex

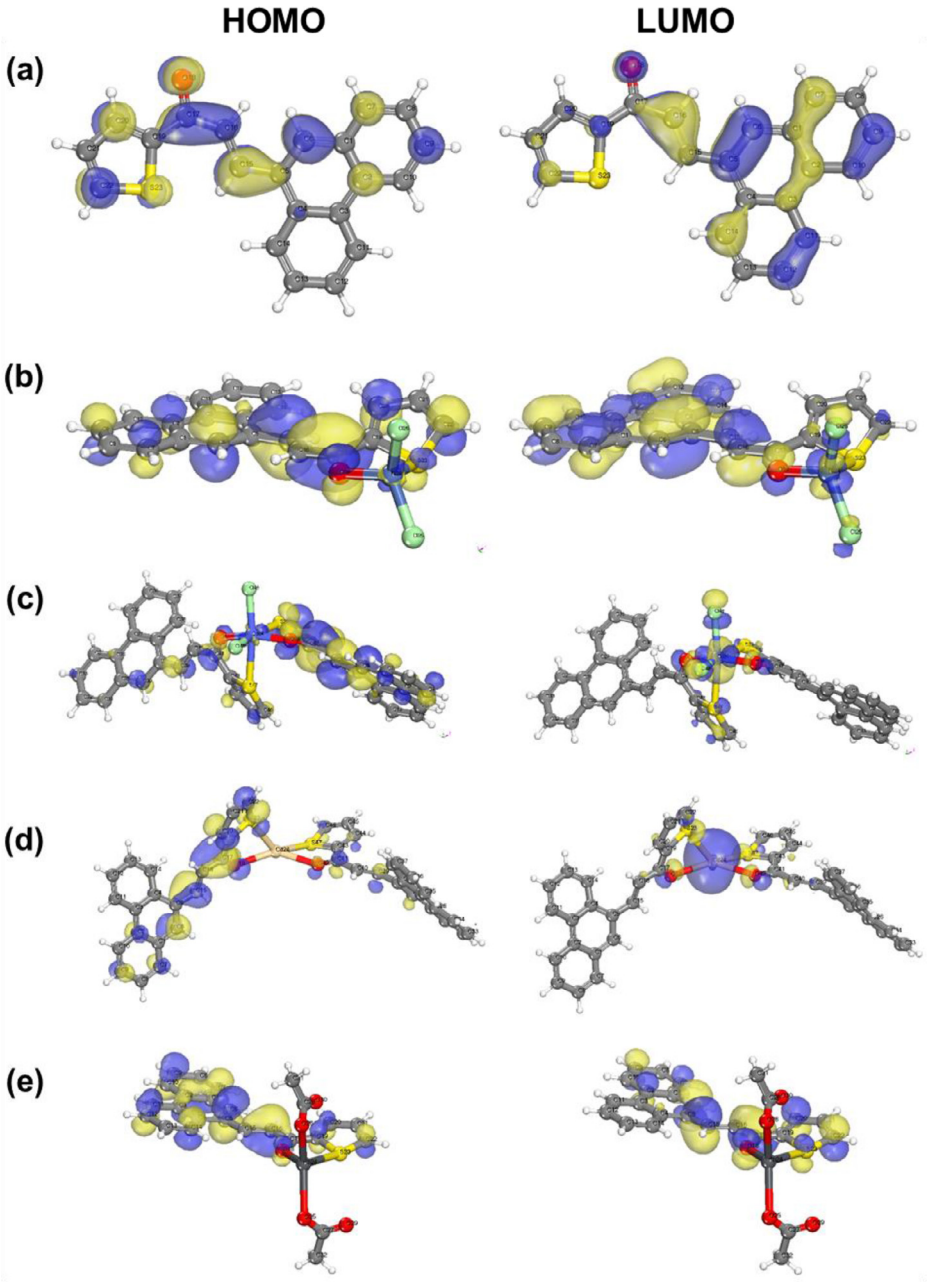

Fig. 12. The HOMO and LUMO of (a) **PhTPO**, (b) [**PhTPO-**Ni^{2+}], (c) [**PhTPO-**Co^{2+}], (d) [**PhTPO-**Cd^{2+}], and (e) [**PhTPO-**Pd^{2+}].

Table 7
Calculated E_{HOMO}, E_{LUMO}, energy band gap (E_H – E_L), electronegativity (χ), chemical potential (μ), global hardness (η), global softness (S), global electrophilicity index (ω) reactivity index (ΔN_{max}) for **PhTPO** and its complexes.

Compound	E_H (eV)	E_L (eV)	(E_H -E_L) (eV)	χ (eV)	μ(eV)	η (eV)	S (eV^{-1})	ω(eV)	σ (eV)	ΔN_{max}
PhTPO	−5.113	−3.271	1.842	4.192	−4.192	0.921	0.461	9.540	1.086	4.55157
[**PhTPO-**Co^{2+}]	−4.292	−3.187	1.105	3.740	−3.740	0.553	0.276	12.655	1.810	6.76832
[**PhTPO-**Ni^{2+}]	−5.048	−3.264	1.784	4.156	−4.156	0.892	0.446	9.682	1.121	4.65919
[**PhTPO-**Pb^{2+}]	−5.14	−3.317	1.823	4.229	−4.229	0.912	0.456	9.808	1.097	4.63905
[**PhTPO-**Cd^{2+}]	−3.92	−2.966	0.954	3.443	−3.443	0.477	0.239	12.426	2.096	7.21802

had a greater value (7.21802 eV) than **PhTPO** ligand and other complexes which concluded that Cd^{2+} complex had a higher electrons acceptance system (electrophiles). (5) Calculations of the values of the energy component (Table S3) reveals that the increase in the value of the evaluated binding energy of the complexes compared to that of the ligand indicates the stability of the investigated metal complexes.

3.7. Biological studies

In Vitro cytotoxic activity of **PhTPO** and its Co^{2+}, Ni^{2+}, Pb^{2+}, and Cd^{2+} complexes against four different human tumor cell lines HePG-2, MCF-7, PC3 and HCT-116 was tested using a colorimetric assay (MTT assay). The cytotoxicity results were described by growth inhibitory concentration value (IC_{50}), which means the

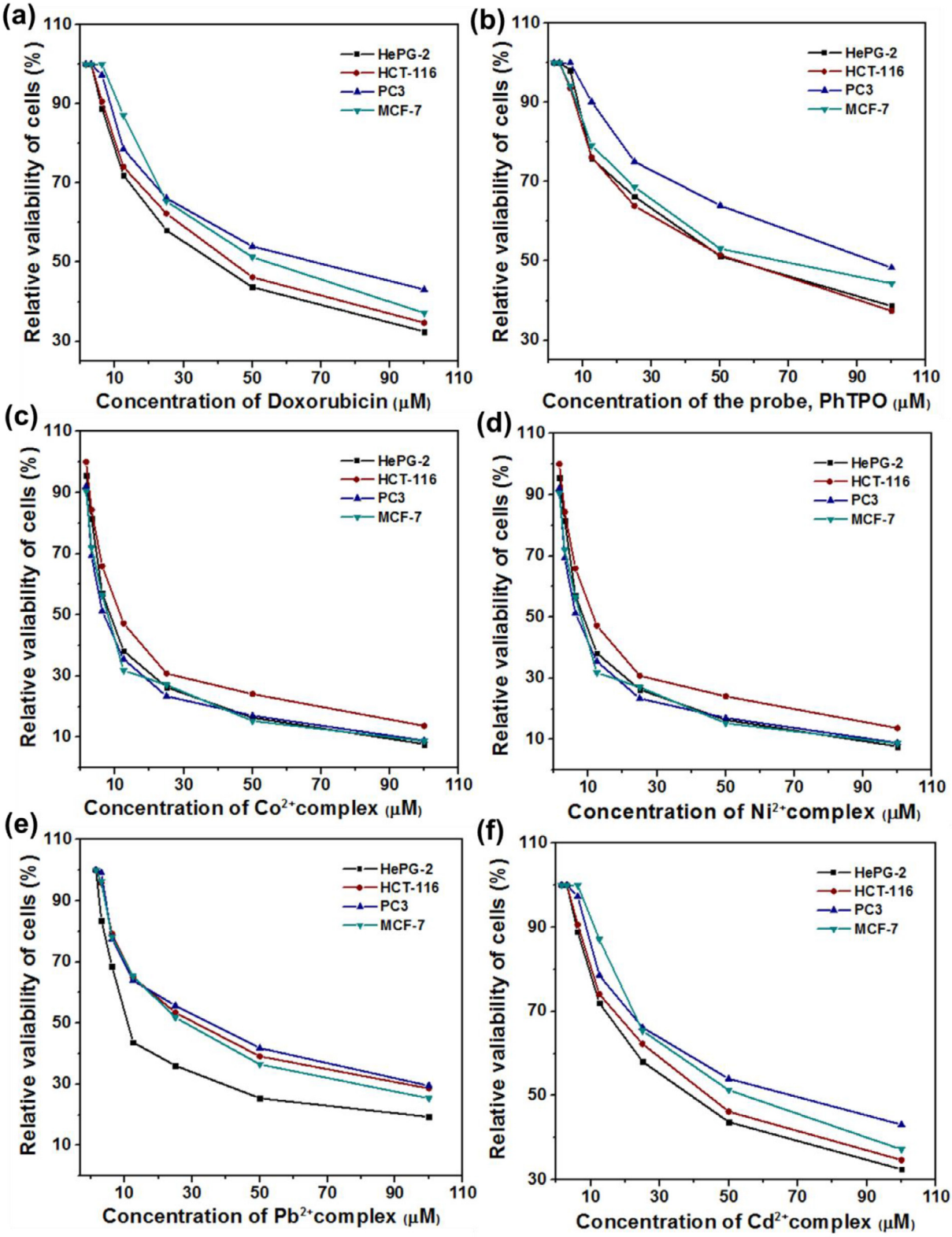

Fig. 13. Survival curve of the tumor cell line; (a) Doxorubicin, (b) **PhTPO**, (c) [**PhTPO-**Co^{2+}], (d) [**PhTPO-**Ni^{2+}], (e) [**PhTPO-**Pb^{2+}], and (f) [**PhTPO-**Cd^{2+}].

concentration of the compounds required to reach a 50% inhibition of cell growth after incubation for 72 h, parallel to untreated controls. The IC_{50} values were calculated from the survival curve of the tumor cell line which was plotted between concentration and% cell viability. A wide range of different concentrations of each test compound (1.56, 3.125, 6.25, 12.5, 25, 50 and 100 μM) was established in Fig. 13 and the data were summarized in Table S4.

The results of IC_{50} concentrations of the synthesized compounds parallel to the vastly utilized anticancer drug, Doxorubicin as standard were presented in Table 8. Each data point was an average of three independent experiments and expressed as the

Table 8
Cytotoxic activity of **PhTPO** and [**PhTPO-**M] complexes against human tumor cells.

Compound	*In vitro* Cytotoxicity IC_{50} (μM) *			
	HePG2	HCT-116	PC3	MCF-7
DOX	4.50 ± 0.3	5.23 ± 0.2	8.87 ± 0.6	4.17 ± 0.2
PhTPO	54.72 ± 3.5	52.53 ± 3.4	87.16 ± 4.9	64.95 ± 3.8
[**PhTPO-**Co^{2+}]	9.86 ± 0.9	22.45 ± 2.0	20.39 ± 1.8	17.54 ± 1.5
[**PhTPO-**Ni^{2+}]	9.44 ± 0.8	13.05 ± 1.2	7.62 ± 0.6	8.02 ± 0.7
[**PhTPO-**Pb^{2+}]	14.14 ± 1.2	30.68 ± 2.6	32.73 ± 2.8	28.03 ± 2.3
[**PhTPO-**Cd^{2+}]	20.73 ± 3.0	40.12 ± 3.1	45.70 ± 3.7	35.09 ± 3.6

***IC_{50} (μM):** 1 – 10 (very strong). 11 – 20 (strong). 21 – 50 (moderate). 51 – 100 (weak), and above 100 (non-cytotoxic).
****DOX** = Doxocubicin.

Table 9
Anti-oxidant assays by erythrocyte hemolysis (A/B x 100).

Compound	Erythrocyte hemolysis A/B x 100	
	Absorbance of samples (A)	% Hemolysis
H_2O (B)	0.846	–
Vitamin-c	0.035	4.1%
PhTPO	0.056	6.6%
[**PhTPO-**Co^{2+}]	0.039	4.6%
[**PhTPO-**Ni^{2+}]	0.038	4.5%
[**PhTPO-**Pb^{2+}]	0.043	5.1%
[**PhTPO-**Cd^{2+}]	0.052	6.1%

Table 10
Anti-oxidant assays by ABTS method [($Abs_{control}$-Abs_{test})/$Abs_{control}$ x 100].

Compounds	Absorbance of samples	% inhibition
Control of ABTS	0.498	0%
Ascorbic-acid	0.057	88.5%
PhTPO	0.415	16.7%
[**PhTPO-**Co^{2+}]	0.371	25.5%
[**PhTPO-**Ni^{2+}]	0.367	26.3%
[**PhTPO-**Pb^{2+}]	0.384	22.9%
[**PhTPO-**Cd^{2+}]	0.402	19.3%

value ± SD. **PhTPO** showed a weak cytotoxic activity compared to the metal complexes Co^{2+}, Ni^{2+}, Pb^{2+}, and Cd^{2+}, indicating that probe clearly gave fewer effective compounds against the tumor cell lines. [**PhTPO-**Ni^{2+}] and [**PhTPO-**Co^{2+}] showed a better cytotoxic activity than the other metal complexes as well as the investigated probe. The order of activity is found to be [**PhTPO-**Ni^{2+}]> [**PhTPO-**Co^{2+}]> [**PhTPO-**Pb^{2+}]> [**PhTPO-**Cd^{2+}]> **PhTPO**. The obtained results suggested that such metal complexes could be used in the designing and improvement of new anticancer drugs. The activity might be correlated with the strength of the M-L bond, as well as other variables like cation size, diffusion, receptor sites, and a combination of the metal and ligand for biomolecule [74].

The antioxidant assay of **PhTPO** and its complexes were evaluated by two *in vitro* methods in order to compare the results erythrocyte hemolysis, Table 9 and ABTS method, Table 10. The results showed that **PhTPO** has a weak anti-oxidative activity, while [**PhTPO-**Ni^{2+}] exhibited a potent activity, compared to the other metal complexes. The order of antioxidant activity for the metal complexes was found to be [**PhTPO-Ni^{2+}**]> [**PhTPO-Co^{2+}**]> [**PhTPO-Pb^{2+}**]> [**PhTPO-Cd^{2+}**]> **PhTPO**.

3.8. Molecular docking

It is recognized that molecular docking has high significance in the discovery of drugs. The 3W2S of EGFR was docked the invesigated compounds with the most favorable active site (LEU 718, VAL 726, LYS 745, ALA 722, GLY 719, ARG 841, ASP 855, and PHE 723) of 3W2S that predicted by the site-finder algorithm in MOE. Depending on the S-score, the largest docking pocket was assigned and all hits were docked against the most active site using the MOE docking software, Table 11. For further evaluation, the best docked hit compounds with higher S-score and lower RMSD values were identified. Based on the results tabulated, it can be deduced that the Cd^{2+} complex has the lowest inhibitory activity of the EGFR protein. The ligand, **PhTPO** and its metal complexes' inhibitory activity were compared on the basis of S-score values exhibiting that the order of inhibitory activity to the EGFR protein is found to be [**PhTPO-**Co^{2+}]>**PhTPO** > [**PhTPO-**Pb^{2+}] >[**PhTPO-**Ni^{2+}] > [**PhTPO-**Cd^{2+}]. According this order, [**PhTPO-**Co^{2+}] complex shows the highest inhibitory activity to the EGFR protein similar to the experimental anticancer data. It is noted that the weak π-Hydrogen donor contacts are most frequent type of interactions between **PhTPO** and its complexes with EGFR receptor. In the case of EGFR-**PhTPO** (Fig. 14), 6-membered rings of **PhTPO** builds π-H interaction with LEU 718 and VAL 726 of EGFR (with distances 4.29, and 4.53 Å, respectively). While, [**PhTPO-**Co^{2+}] shows hydrogen acceptor interaction of chloride atom of [**PhTPO-**Co^{2+}] complex with amino acids GLY 719 and ALA 722 (distance = 3.72 and 3.35 Å) in addition to π-H interaction of LEU 718 with 6-membered rings of **PhTPO**.

The molecular docking result for the interactions of remaining complexes, Figure S9-S12, with the EGFR protein shows that the dominant types of interactions are hydrophobic interactions, such as π-H, In addition, an ionic interaction of sulfur atom of [**PhTPO-**Pb^{2+}] complex with amino acid ASP 855 as well as an ionic interaction of Cd-ion of [**PhTPO-**Cd^{2+}] complex with amino acid LYS 745. Moreover, the hydrogen acceptor bonds of amino acids LYS 745 with the chloride atom of [**PhTPO-**Ni^{2+}] complex and the oxygen atom of [**PhTPO-**Cd^{2+}] complex. Finally, the ASP 855 of EGFR shows hydrogen donor bond with carbon atom of the aromatic ring of [**PhTPO-**Pb^{2+}].

Table 11
Molecular docking scoring, RMSD, interaction results of the investigated compounds

Compounds	S	RMSD	interaction	Receptor	Distance (Å)
PhTPO	-6.91364	0.9446	π-H	LEU 718	4.29
			π-H	VAL 726	4.53
[**PhTPO-**Co^{2+}]	-7.87406	1.2420	H-acceptor	GLY 719	3.72
			H-acceptor	ALA 722	3.35
			π-H	LEU 718	3.99
[**PhTPO-**Ni^{2+}]	-5.43354	1.3768	H-acceptor	LYS 745	4.08
[**PhTPO-**Pb^{2+}]	-6.25821	1.5994	H-donor	ASP 855	2.80
			Ionic	ASP 855	3.18
[**PhTPO-**Cd^{2+}]	-3.03933	1.4156	H-acceptor	LYS 745	2.77
			Ionic	LYS 745	3.53
			π-H	LEU 718	4.02

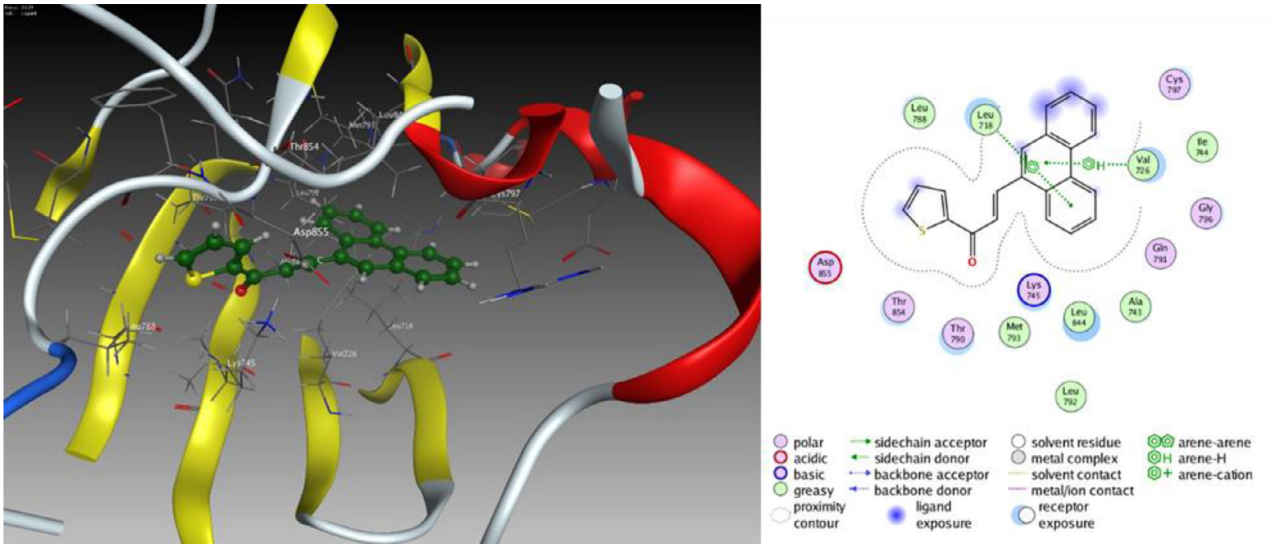

Fig. 14. 3D and 2D molecular interaction of **PhTPO** to inhibitory activity to the EGFR protein.

4. Conclusions

D–π–A optical probe composed polycyclic aromatic and thiophene moieties was successfully synthesized and characterized. The solvatochromic response was investigated in different solvents of various polarities. Also, its optical sensing response to H^+ proton and metal ions was investigated. The absorption and emission spectra are sensitive towards H^+proton owing to acidochromic behavior. The absorption spectra of the investigated probe changed dramatically upon increasing the concentration of sulfuric acid with an observable change in color. Also, it is responsive to the tested metal ions and show significant change in both absorption and emission spectra upon adding different concentrations of the metal salts confirming the intramolecular charge transfer of the probe upon effective coordination with the used metal ions. These spectral changes suggest that the investigated probe would be potential candidate for environmental polarity, and sensor for H^+ proton and metal ions and. Solid Co^{2+}, Ni^{2+}, $Pb^{2+}$and Cd^{2+} complexes were also synthesized and characterized. Depending on the magnetic moments results, the geometric structures were found to be octahedral and tetrahedral for paramagnetic Co^{2+}, and Ni^{2+} complexes, respectively, while, they are diamagnetic for Pb^{2+} and Cd^{2+} complexes. The biological activity shows potent cytotoxic and anticancer activity which suggest the obtained complexes are good candidate for further antitumor activities studies. From molecular docking interaction, [**PhTPO-**Co^{2+}] complex shows the highest inhibitory activity to the EGFR protein similar to the experimental anticancer data with S score value equals −7.87406 and RMSD value equals 1.2420.

CRedit authorship contribution statement

Dr. Marwa N. El-Nahass: Conceptualization, Methodology, Software, Investigation, Writing-review, editing, Data curation, Formal analysis.

Finally, the responsible for communicating with the journal and sending the research paper.

Prof. Dr. Tarek A. Fayed:

Put and discuss the research idea, enhance the literature survey, revised the paper before and after sending.

Prof. Dr. Saleh Abd Elazim: Put and discuss the research idea.

Doaa Fawzy: Methodology, Writing & editing, Data curation, Formal analysis.

Dr. Fathy Hassan: Contribute to refine the manuscript. Software, contribute in editing, Data curation, Formal analysis.

Declaration of Competing Interest

The authors declare that they have no known competing financial interests or personal relationships that could have appeared to influence the work reported in this paper.

Supplementary materials

Supplementary material associated with this article can be found, in the online version, at doi:10.1016/j.molstruc.2021.130581.

References

[1] A.S. Klymchenko, Solvatochromic and fluorogenic dyes as environment-sensitive probes: design and biological applications, Acc. Chem. Res. 50 (2) (2017) 366–375, doi:10.1021/acs.accounts.6b00517.
[2] B. Carlotti, A. Cesaretti, O. Cannelli, T. Giovannini, C. Cappelli, C. Bonaccorso, C.G. Fortuna, F. Elisei, A. Spalletti, Evaluation of hyperpolarizability from the solvatochromic method: thiophene containing push–pull cationic dyes as a case study, J. Phys. Chem. C 122 (4) (2018) 2285–2296, doi:10.1021/acs.jpcc.7b10647.
[3] E.V. Verbitskiy, E.M. Cheprakova, J.O. Subbotina, A.V. Schepochkin, P.A. Slepukhin, G.L. Rusinov, V.N. Charushin, O.N. Chupakhin, N.I. Makarova, A.V. Metelitsa, Synthesis, spectral and electrochemical properties of pyrimidine-containing dyes as photosensitizers for dye-sensitized solar cells, Dyes Pigment. 100 (2014) 201–214, doi:10.1016/j.dyepig.2013.09.006.
[4] P. Bamfield, The Royal Society of Chemistry, Cambridge, 2001.
[5] M.C. Janzen, J.B. Ponder, D.P. Bailey, C.K. Ingison, K.S. Suslick, Colorimetric sensor arrays for volatile organic compounds, Anal. Chem. 78 (11) (2006) 3591–3600, doi:10.1021/ac052111s.
[6] V. Antonov, K. Hohla, Dye stability under excimer-laser pumping, Appl. Phys. B 30 (3) (1983) 109–116, doi:10.1007/BF00695464.
[7] S. Speiser, N. Shakkour, Photoquenching parameters for commonly used laser dyes, Appl. Phys. B 38 (3) (1985) 191–197, doi:10.1007/BF00697483.
[8] A.P. De Silva, H.N. Gunaratne, T. Gunnlaugsson, A.J. Huxley, C.P. McCoy, J.T. Rademacher, T.E. Rice, Signaling recognition events with fluorescent sensors and switches, Chem. Rev. 97 (5) (1997) 1515–1566, doi:10.1021/cr960386p.
[9] D. Zhang, Q. Zhang, J. Su, H. Tian, A dual-ion-switched molecular brake based on ferrocene, Chem. Commun. (13) (2009) 1700–1702, doi:10.1039/b823073k.
[10] J. Sansregret, J. Drake, W. Thomas, M. Lesiecki, Light transport in planar luminescent solar concentrators: the role of DCM self-absorption, Appl. Opt. 22 (4) (1983) 573–577, doi:10.1364/AO.22.000573.
[11] B. Liu, W. Zhu, Q. Zhang, W. Wu, M. Xu, Z. Ning, Y. Xie, H. Tian, Conveniently synthesized isophorone dyes for high efficiency dye-sensitized solar cells: tuning photovoltaic performance by structural modification of donor group in donor–π–acceptor system, Chem. Commun. (13) (2009) 1766–1768, doi:10.1039/b820964b.
[12] X. Zhang, B. Chen, X. Lin, O. Wong, C. Lee, H. Kwong, S. Lee, S. Wu, A new family of red dopants based on chromene-containing compounds for

organic electroluminescent devices, Chem. Mater. 13 (5) (2001) 1565–1569, doi:10.1021/cm0008664.
[13] Y. Wei, G. Qin, W. Wang, W. Bian, S. Shuang, C. Dong, Development of fluorescent FeIII sensor based on chalcone, J. Lumin. 131 (8) (2011) 1672–1676, doi:10.1016/j.jlumin.2011.03.062.
[14] J. Wu, W. Liu, J. Ge, H. Zhang, P. Wang, New sensing mechanisms for design of fluorescent chemosensors emerging in recent years, Chem. Soc. Rev. 40 (7) (2011) 3483–3495, doi:10.1039/c0cs00224k.
[15] R. Kumari, A. Varghese, L. George, Y. Sudhakar, Effect of solvent polarity on the photophysical properties of chalcone derivatives, RSC Adv. 7 (39) (2017) 24204–24214, doi:10.1039/C7RA01705G.
[16] S. Prabu, R. Nagalakshmi, P. Srinivasan, Investigations on the physico chemical properties of 4-bromochalcone single crystals for nonlinear optical applications, Spectrochim. Acta Part A Mol. Spectrosc. 103 (2013) 45–52, doi:10.1016/j.saa.2012.10.073.
[17] Y. Sato, M. Morimoto, H. Segawa, T. Shimidzu, Twisted intramolecular charge-transfer state of a donor-acceptor molecular system with a. beta.-Diketone bridge: tuning of emission through structural restriction by metal cation coordination, J. Phys. Chem. 99 (1) (1995) 35–39, doi:10.1021/j100001a007.
[18] T.A. Fayed, M.A. El-Morsi, M.N. El-Nahass, Intramolecular charge transfer emission of a new ketocyanine dye: effects of hydrogen bonding and electrolyte, J. Photochem. Photobiol. A Chem. 224 (1) (2011) 38–45, doi:10.1016/j.jphotochem.2011.09.004.
[19] S. Shaily, A. Kumar, N. Ahmed, A coumarin–chalcone hybrid used as a selective and sensitive colorimetric and turn-on fluorometric sensor for Cd 2+ detection, New J. Chem. 41 (23) (2017) 14746–14753, doi:10.1039/C7NJ02569F.
[20] D.M. Shin, D.M. Song, K.H. Jung, J.H. Moon, Photochemical transformation of chalcone derivatives, J. Photosci. 8 (1) (2001) 9–12.
[21] H.K. Hsieh, T.H. Lee, J.P. Wang, J.J. Wang, C.N. Lin, Synthesis and anti-inflammatory effect of chalcones and related compounds, Pharm. Res. 15 (1) (1998) 39–46, doi:10.1023/A:1011940401754.
[22] M.L. Bello, L.D. Chiaradia, L.R.S. Dias, L.K. Pacheco, T.R. Stumpf, A. Mascarello, M. Steindel, R.A. Yunes, H.C. Castro, R.J. Nunes, Trimethoxy-chalcone derivatives inhibit growth of Leishmania braziliensis: synthesis, biological evaluation, molecular modeling and structure–activity relationship (SAR), Biorg. Med. Chem. 19 (16) (2011) 5046–5052, doi:10.1016/j.bmc.2011.06.023.
[23] T.H. Bui, N.T. Nguyen, P.H. Dang, H.X. Nguyen, M.T.T. Nguyen, Design and synthesis of chalcone derivatives as potential non-purine xanthine oxidase inhibitors, Springerplus 5 (1) (2016) 1–8, doi:10.1186/s40064-016-3485-6.
[24] O. Mesenzani, A. Massarotti, M. Giustiniano, T. Pirali, V. Bevilacqua, A. Caldarelli, P. Canonico, G. Sorba, E. Novellino, A.A. Genazzani, Replacement of the double bond of antitubulin chalcones with triazoles and tetrazoles: synthesis and biological evaluation, Bioorg. Med. Chem. Lett. 21 (2) (2011) 764–768, doi:10.1016/j.bmcl.2010.11.113.
[25] M.N. El-Nahass, D.M. Abd El-Aziz, T.A. Fayed, Selective “on–off–on” switchable chemosensor for metal ions detection and its complexes, Sens. Actuators B Chem. 205 (2014) 377–390, doi:10.1016/j.snb.2014.08.067.
[26] M.N. El-Nahass, T.A. Fayed, M.H. Shaaban, F.M. Hassan, Chalcone isothiocyanate-mesoporous silicates: selective anchoring and toxic metal ions detection, Sens. Actuators B Chem. 210 (2015) 56–68, doi:10.1016/j.snb.2014.12.079.
[27] M.N. El-Nahass, T.A. Fayed, Chemosensing hybrid materials: chalcones-functionalized cage-like mesoporous SBA-16 material for highly selective detection of toxic metal ions, Appl. Organomet. Chem. 31 (11) (2017) e3751, doi:10.1002/aoc.3751.
[28] T.A. Fayed, M.H. Shaaban, M.N. El-Nahass, F.M. Hassan, Chalcones isothiocyanate anchored into mesoporous silicate: synthesis, characterization and metal ions sensing response, Microporous Mesoporous Mater. 198 (2014) 144–152, doi:10.1016/j.micromeso.2014.07.031.
[29] A. Floyd, S. Dyke, S. Ward, The synthesis of phenanthrenes, Chem. Rev. 76 (5) (1976) 509–562, doi:10.1021/cr60303a001.
[30] G.H. Jeffery, J. Bassett, J. Mendham, R.C. Denney, Vogel'sTextbook of Quantitative Chemical Analysis, John Wiley & Sons, Inc., New York, 1989.
[31] G.A. Crosby, J.N. Demas, Measurement of photoluminescence quantum yields. Review, J. Phys. Chem. 75 (8) (1971) 991–1024, doi:10.1021/j100678a001.
[32] K. Prasanth, R.S. Pillai, S.A. Peter, H. Bajaj, R. Jasra, H. Chung, T. Kim, S. Song, Hydrogen uptake in palladium and ruthenium exchanged zeolite X, J. Alloy. Compd. 466 (1–2) (2008) 439–446, doi:10.1016/j.jallcom.2007.11.058.
[33] Modeling and Simulation Solutions For Chemicals and Materials Research, BIOVIA Materials Studio, Accelrys software Inc., San Diego, USA, 2017.
[34] X. Wu, A.K. Ray, Density-functional study of water adsorption on the PuO 2 (110) surface, Phys. Rev. B 65 (8) (2002) 085403, doi:10.1103/PhysRevB.65.085403.
[35] B. Delley, From molecules to solids with the DMol 3 approach, J. Chem. Phys. 113 (18) (2000) 7756–7764, doi:10.1063/1.1316015.
[36] A. Matveev, M. Staufer, M. Mayer, N. Rösch, Density functional study of small molecules and transition-metal carbonyls using revised PBE functionals, Int. J. Quantum Chem. 75 (4–5) (1999) 863–873, doi:10.1002/(SICI)1097-461X(1999)75:4/5)863::AID-QUA51(3.0.CO;2-T.
[37] B. Delley, D. Ellis, A. Freeman, E. Baerends, D. Post, Binding energy and electronic structure of small copper particles, Phys. Rev. B 27 (4) (1983) 2132, doi:10.1103/PhysRevB.27.2132.
[38] B. Delley, An all-electron numerical method for solving the local density functional for polyatomic molecules, J. Chem. Phys. 92 (1) (1990) 508–517, doi:10.1063/1.458452.
[39] B. Hammer, L.B. Hansen, J.K. Nørskov, Improved adsorption energetics within density-functional theory using revised Perdew-Burke-Ernzerhof functionals, Phys. Rev. B 59 (11) (1999) 7413, doi:10.1103/PhysRevB.59.7413.
[40] T. Mosmann, Rapid colorimetric assay for cellular growth and survival: application to proliferation and cytotoxicity assays, J. Immunol. Methods 65 (1–2) (1983) 55–63, doi:10.1016/0022-1759(83)90303-4.
[41] F. Denizot, R. Lang, Rapid colorimetric assay for cell growth and survival: modifications to the tetrazolium dye procedure giving improved sensitivity and reliability, J. Immunol. Methods 89 (2) (1986) 271–277, doi:10.1016/0022-1759(86)90368-6.
[42] E.A. Lissi, B. Modak, R. Torres, J. Escobar, A. Urzua, Total antioxidant potential of resinous exudates from Heliotropium species, and a comparison of the ABTS and DPPH methods, Free Radical Res. 30 (6) (1999) 471–477, doi:10.1080/10715769900300511.
[43] A.B.A. El-Gazzar, M.M. Youssef, A.M.S. Youssef, A.A. Abu-Hashem, F.A. Badria, Design and synthesis of azolopyrimidoquinolines, pyrimidoquinazolines as anti-oxidant, anti-inflammatory and analgesic activities, Eur. J. Med. Chem. 44 (2) (2009) 609–624, doi:10.1016/j.ejmech.2008.03.022.
[44] R. Aeschbach, J. Löliger, B.C. Scott, A. Murcia, J. Butler, B. Halliwell, O.I. Aruoma, Antioxidant actions of thymol, carvacrol, 6-gingerol, zingerone and hydroxytyrosol, Food Chem. Toxicol. 32 (1) (1994) 31–36, doi:10.1016/0278-6915(84)90033-4.
[45] Y. Morimoto, K. Tanaka, Y. Iwakiri, S. Tokuhiro, S. Fukushima, Y. Takeuchi, Protective effects of some neutral amino acids against hypotonic hemolysis, Biol. Pharm. Bull. 18 (10) (1995) 1417–1422, doi:10.1248/bpb.18.1417.
[46] O.A. El-Gammal, G.M. Abu El-Reash, M.M. El-Gamil, Structural, spectral, pH-metric and biological studies on mercury (II), cadmium (II) and binuclear zinc (II) complexes of NS donor thiosemicarbazide ligand, Spectrochim. Acta Part A Mol. Spectrosc. 123 (2014) 59–70, doi:10.1016/j.saa.2013.12.034.
[47] E.H. Avdović, Ž.B. Milanović, M.N. Živanović, D.S. Šeklić, I.D. Radojević, L.R. Čomić, S.R. Trifunović, A. Amić, Z.S. Marković, Synthesis, spectroscopic characterization, biological activity, DFT and molecular docking study of novel 4-hydroxycoumarine derivatives and corresponding palladium (II) complexes, Inorg. Chim. Acta 504 (2020) 119465, doi:10.1016/j.ica.2020.119465.
[48] Integrated Computer-Aided Molecular Design Platform, Molecular operating Environment, Chemical Computing Group, 2019.
[49] R. Shah, A. Alharbi, A.M. Hameed, F. Saad, R. Zaky, A.M. Khedr, N. El-Metwaly, Synthesis and structural elucidation for new schiff base complexes; conductance, conformational, MOE-docking and biological studies, J. Inorg. Organomet. Polym. Mater. 30 (9) (2020) 3595–3607, doi:10.1007/s10904-020-01505-w.
[50] S. Sogabe, Y. Kawakita, S. Igaki, H. Iwata, H. Miki, D.R. Cary, T. Takagi, S. Takagi, Y. Ohta, T. Ishikawa, Structure-based approach for the discovery of pyrrolo [3, 2-d] pyrimidine-based EGFR T790M/L858R mutant inhibitors, ACS Med. Chem. Lett. 4 (2) (2013) 201–205, doi:10.1021/ml300327z.
[51] M.T. ul Qamar, S. Kiran, U.A. Ashfaq, M.R. Javed, F. Anwar, M.A. Ali, A.u.H. Gilani, Discovery of novel dengue NS2B/NS3 protease inhibitors using pharmacophore modeling and molecular docking based virtual screening of the zinc database, Inter. J. Pharm. 12 (6) (2016) 621–632.
[52] N.G. Bakshiev, Universal intermolecular interactions and their effect on the position of the electronic spectra of molecules in two component solutions„ Opt. Spektrosk. 16 (1964) 821–832.
[53] O. Ermer, in: Calculation of Molecular Properties Using Force fields. Applications in Organic chemistry, Bonding forces, Springer, 1976, pp. 161–211.
[54] J. Barriga, B. Coto, B. Fernandez, Molecular dynamics study of optimal packing structure of OTS self-assembled monolayers on SiO_2 surfaces, Tribol. Int. 40 (6) (2007) 960–966, doi:10.1016/j.triboint.2006.02.030.
[55] K. Khaled, Monte Carlo simulations of corrosion inhibition of mild steel in 0.5M sulphuric acid by some green corrosion inhibitors, J. Solid State Electrochem. 13 (11) (2009) 1743–1756, doi:10.1007/s10008-009-0845-y.
[56] K. Khaled, S.A. Fadl-Allah, B. Hammouti, Some benzotriazole derivatives as corrosion inhibitors for copper in acidic medium: experimental and quantum chemical molecular dynamics approach, Mater. Chem. Phys. 117 (1) (2009) 148–155, doi:10.1016/j.matchemphys.2009.05.043.
[57] C. von Bültzingslöwen, A.K. McEvoy, C. McDonagh, B.D. MacCraith, I. Klimant, C. Krause, O.S. Wolfbeis, Sol-gel based optical carbon dioxide sensor employing dual luminophore referencing for application in food packaging technology, Analyst 127 (11) (2002) 1478–1483, doi:10.1039/B207438A.
[58] V.F. Curto, S. Coyle, R. Byrne, N. Angelov, D. Diamond, F. Benito-Lopez, Concept and development of an autonomous wearable micro-fuidic platform for real time pH sweat analysis, Sens. Actuator B Chem. 175 (2012) 263–270, doi:10.1016/j.snb.2012.02.010.
[59] B. Kuswandi, Jayus, T.S. Larasati, A. Abdullah, L.Y. Heng, Real-time monitoring of shrimp spoilage using on-package sticker sensor based on natural dye of curcumin, Food Anal. Methods 5 (4) (2012) 881–889, doi:10.1007/s12161-011-9326-x.
[60] L. Van der Schueren, K. De Clerck, Coloration and application of pH-sensitive dyes on textile materials, Color Technol. 128 (2) (2012) 82–90, doi:10.1111/j.1478-4408.2011.00361.x.
[61] M.B. Mikkelsen, R. Marie, J.H. Hansen, D. Wencel, C. McDonagh, H.O. Nielsen, A. Kristensen, Controlled deposition of sol-gel sensor material using hemiwicking, J. Micromech. Microeng. 21 (11) (2011) 115008 https://10.1088/0960-1317/21/11/115008.
[62] H.A. Benesi, J. Hildebrand, A spectrophotometric investigation of the interaction of iodine with aromatic hydrocarbons, J. Am. Chem. Soc. 71 (8) (1949) 2703–2707, doi:10.1021/ja01176a030.

[63] A.S. Hill, M.J. Friedman, S.H. Reiber, G.V. Korshin, R.L. Valentine, Behavior of trace inorganic contaminants in drinking water distribution systems, J. Am. Water Works Assoc. 102 (7) (2010) 107–118, doi:10.1002/j.1551-8833.2010.tb10153.x.
[64] L. Basabe-Desmonts, D.N. Reinhoudt, M.J. Crego-Calama, Design of fuorescent materials for chemical sensing, Chem. Soc. Rev. 36 (6) (2007) 993–1017, doi:10.1039/B609548H.
[65] M. Tian, L. Fang, X. Yan, W. Xiao, K.H. Row, Determination of heavy metal ions and organic pollutants in water samples using ionic liquids and ionic liquid-modified sorbents, J. Anal. Methods Chem. 2019 (2019) 19 Article ID 1948965, doi:10.1155/2019/1948965.
[66] S.S. Kandil, G.B. El-Hefnawy, E.A. Baker, Thermal and spectral studies of 5-(phenylazo)-2-thiohydantoin and 5-(2-hydroxyphenylazo)-2-thiohydantoin complexes of cobalt (II), nickel (II) and copper (II), Thermochim. Acta 414 (2) (2004) 105–113, doi:10.1016/j.tca.2003.11.021.
[67] S.S. Kandil, G.B. El-Hefnawy, E.A. Bakr, A.Z. Abou El-Ezz, Cobalt (II), nickel (II) and copper (II) complexes of 5-(2-carboxyphenylazo)-2-thiohydantoin, Transit. Met. Chem. 28 (2) (2003) 168–175, doi:10.1023/A:1022968604281.
[68] Z.A. El-Shafiey, Z. Abd El-Wahab, A. Salman, R. Taha, Study of binary and ternary complexes of Co (II), Ni (II), Cd (II), Fe (III), and UO2 (II) complexes of amino carboxylic acid derivatives and pyridine, synthesis, spectroscopic characterization, thermal investigation and biological activity, Egypt. J. Chem. 53 (2) (2010) 177–202.
[69] C.M. Da Silva, D.L. da Silva, L.V. Modolo, R.B. Alves, M.A. de Resende, C.V. Martins, Â.de Fátima, Schiff bases: a short review of their antimicrobial activities, J. Adv. Res. 2 (1) (2011) 1–8, doi:10.1016/j.jare.2010.05.004.
[70] S. Sagdinc, B. Köksoy, F. Kandemirli, S.H. Bayari, Theoretical and spectroscopic studies of 5-fluoro-isatin-3-(N-benzylthiosemicarbazone) and its zinc (II) complex, J. Mol. Struct. 917 (2–3) (2009) 63–70, doi:10.1016/j.molstruc.2008.06.033.
[71] R.G. Pearson, Absolute electronegativity and hardness: applications to organic chemistry, J. Org. Chem. 54 (6) (1989) 1423–1430, doi:10.1021/jo00267a034.
[72] G. Abu El-Reash, O. El-Gammal, S. Ghazy, A. Radwan, Characterization and biological studies on Co (II), Ni (II) and Cu (II) complexes of carbohydrazones ending by pyridyl ring, Spectrochim. Acta Part A Mol. Spectrosc. 104 (2013) 26–34, doi:10.1016/j.saa.2012.11.008.
[73] M. Gaber, T.A. Fayed, M.M. El-Gamil, G.M. Abu El-Reash, Structural, thermogravimetric, B3LYP and biological studies on some heterocyclic thiosemicarbazide copper (II) complexes and evaluation of their molecular docking, J. Mol. Struct. 1151 (2018) 56–72, doi:10.1016/j.molstruc.2017.09.035.
[74] R. Nagar, Syntheses, characterization, and microbial activity of some transition metal complexes involving potentially active O and N donor heterocyclic ligands, J. Inorg. Biochem. 40 (4) (1990) 349–356, doi:10.1016/0162-0134(90)80069-A.